



CALPHAD modeling of the glass transition for a pure substance, coupling thermodynamics and relaxation kinetics

P. Benigni

► To cite this version:

P. Benigni. CALPHAD modeling of the glass transition for a pure substance, coupling thermodynamics and relaxation kinetics. Calphad, 2021, 72, pp.102238. <10.1016/j.calphad.2020.102238>. <hal-03117313>

HAL Id: hal-03117313

<https://hal.science/hal-03117313v1>

Submitted on 21 Jan 2021

HAL is a multi-disciplinary open access archive for the deposit and dissemination of scientific research documents, whether they are published or not. The documents may come from teaching and research institutions in France or abroad, or from public or private research centers.

L'archive ouverte pluridisciplinaire **HAL**, est destinée au dépôt et à la diffusion de documents scientifiques de niveau recherche, publiés ou non, émanant des établissements d'enseignement et de recherche français ou étrangers, des laboratoires publics ou privés.



HAL Authorization

CALPHAD modeling of the glass transition for a pure substance, coupling thermodynamics and relaxation kinetics

P. Benigni, Aix Marseille Univ., Université de Toulon, CNRS, IM2NP, Marseille, France

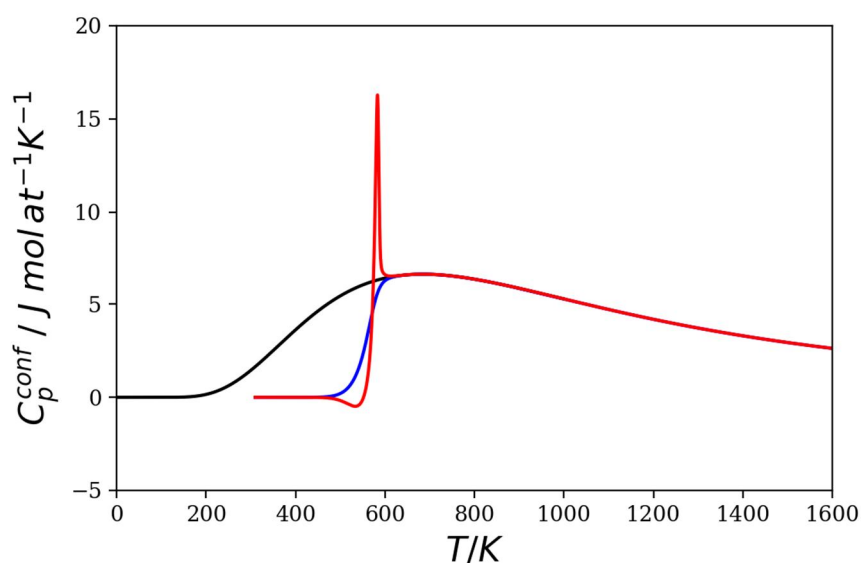
Institut Matériaux Microélectronique Nanosciences de Provence, UMR 7334 CNRS – Aix-Marseille Université, FST St Jérôme, Service 251, avenue Normandie-Niemen, 13397 Marseille – Cedex 20 (France)

Email address: p.benigni@univ-amu.fr

Abstract

A coupled thermodynamic/kinetic CALPHAD type modeling of the glass transition for a glass forming unary substance is proposed. In this quantitative modeling, the vibrational contributions to the thermodynamic functions of the crystal and liquid/glass phases are classically modeled using weighed sums of Einstein functions while the configurational contributions to the liquid/glass phase functions are described using a single internal variable within the frame of the ideal two-state model. The freezing kinetics of this internal variable on cooling is calculated with an Adam-Gibbs logarithmic relaxation law. The model is applied to the boron oxide B_2O_3 and, after a numerical optimization of the parameters, is shown to well represent the hysteresis loop of the heat capacity detected by DSC in the glass transition range during cooling/reheating cycles at various rates. The model also allows to calculate the fictive temperature and residual or zero-point entropy of the glass.

Graphical abstract



Keywords

Thermodynamics; liquid; 2-state model; glass transition; relaxation; boron oxide B_2O_3 .

Introduction

In his classical article from 1948 [1], Kauzmann wrote (page 227): "... a glass is a liquid in which certain degrees of freedom characteristic of liquids are "frozen in" and can no longer contribute to the specific heat and thermal expansion. The problem presented to us by the glassy state is simply to determine what these degrees of freedom are and to explain how they are frozen in at the glass-transformation point". Later in the text (page 229), the author gave the following rewording: "Thus we may define a glass as an amorphous or non-crystalline material in which certain internal degrees of freedom characteristic of the liquid state have not had time to come into thermodynamic equilibrium with their surroundings."

Adopting this view as a roadmap for building a phenomenological CALPHAD modeling of the glass transition for a pure substance, first a thermodynamical model of the liquid/glass phase should be selected. Moreover, this model should be able to describe the stable or metastable equilibrium state of the liquid in term of the external control variables, namely pressure and temperature, and also, at least, one internal variable. Second, the description of the freezing of this (these) internal variable(s) on cooling the liquid requires to couple the thermodynamical model to a kinetic model based on a relaxation law. In this respect, the most natural and general theoretical framework for implementing such modeling is, following Davies and Jones [2] [3], Prigogine and Defay [4], Nemilov [5] and many others, the Thermodynamics of Irreversible Processes (TIP).

Concerning the choice of a thermodynamical model suitable for the coupling, the 1-state models reviewed by Palumbo and Battezzati [6] do not seem to be relevant as they do not feature any internal variable. A bibliography survey covering both the glass research literature and the CALPHAD literature reveals that, as already pointed out by Angell and Rao [7], one key-concept in modeling the transition of a glass to a liquid on heating is to define an excitation of some type. This excitation can be (i) the formation of a hole in the structure, (ii) the increase in the population of a higher energy structural state or (iii) the breaking of a bond.

The first class consists of the lattice-hole models. These models have been used mainly in the glass research community. An introduction to these models can be found in the monograph of Schmelzer and Gutzow [8] and a deeper analysis of the "classical lattice-hole model of liquids" was recently given by the present author [9] where a more extensive bibliography is provided. This type of model, where the internal variable, also called "structural order parameter", represents a fraction of holes present in the quasi-lattice of the liquid, is very close to the CALPHAD approaches used to describe thermal vacancies in crystals such as the one proposed by Guan and Liu [10]. It depicts the glass transition as the freezing of a free volume.

The second class consists of the 2-state models, sometimes also referred to as Two-Level Systems (TLS) in the glass research community. Since the pioneering work of Agren [11] and the subsequent Ringberg Workshops [12] [13], the ideal 2-state model has been adopted and widely used in the CALPHAD community to describe the liquid phase in connection with the development of the so-called "3rd generation databases" e.g. [14]. 2-state models have also been used by glass researchers since a long time e.g. [15]. In these models, the liquid is described as a mixture of two types of structural entities, atoms or molecules, the internal variable being the molar fraction of one or the other type of entities. Interestingly, the coupling of a 2-state model with a relaxation law has already been used by various research groups such as Langer et al. [16] [17], Bisquert et al. [18] [19] [20], Takada et al. [21] and very recently by Jabraoui et al. [22] to study various issues such as the quantitative evaluation of the entropy production during the glass transition and the residual entropy of glasses.

The third class consists of the models based on the "configuron" concept introduced by Angell and Rao [7], where a "configuron" is defined as an elementary configurational excitation associated with the breaking of a chemical bond and its consequences. The Configuron Percolation Theory (CPT) due to Ojovan et al. [23] [24] treats the glass transition as a percolation of broken bonds. Formally, these types of models are also 2-state models, in which the high energy level is the broken bond and the low one the intact bond, operating on a bond lattice instead of the more conventional particle lattice.

In this context, the objective of the present work is to propose a CALPHAD description of the glass

transition for a pure substance, also referred to as a unary in the CALPHAD terminology, by coupling a thermodynamic model with a relaxation law. In agreement with the CALPHAD practice, an ideal 2-state model will be adopted to describe the equilibrium liquid.

Glass research concentrates on a short list of typical glass formers that are extensively investigated by a wide range of complementary experimental techniques. To our knowledge, such elements or substances have not been explored up to now within the frame of the 3rd generation database developments. In the present work, boron oxide B₂O₃ is chosen as a test case of the proposed modeling approach both because of the large amount of experimental information available on this compound and because it is a key component of Pyrex glass and radioactive waste encapsulation borosilicate glasses.

For the sake of simplicity, the scope of the study is reduced to the (T, S) couple of conjugate thermodynamic variables. It is further assumed that, the state of the liquid will depend on only one internal variable, in addition to temperature.

The paper is divided in two main parts.

The first part focuses on the thermodynamic description. A bibliographic overview of several 2-state models is provided in the first subsection. A deeper analysis of the ideal 2-state model is performed in the second subsection. The complete thermodynamic models of the crystal and liquid/glass phases are presented in the third subsection. Experimental information on the thermodynamic properties of B₂O₃ are reviewed in the fourth subsection and the results are presented and discussed in the fifth subsection.

The second part focuses on the kinetic description. Generalities on relaxation phenomena and typical relaxation laws in vitrifying liquids are presented in the first subsection. Issues linked to the implementation and coupling of these laws with the thermodynamic model are dealt with in the second subsection. Experimental data on the relaxation times and relevant law parametrization in B₂O₃ liquid and glass are reviewed in the third subsection. Results of the complete modeling are presented and discussed in the fourth subsection.

Some conclusions and outlooks are given at the end of the paper.

1 Thermodynamic modeling

1.1 Review of various 2-state models

In the simplest version of the 2-state model, the unary liquid is described as an ideal solution of two types of structural entities A and B in chemical equilibrium:



whose corresponding molar fractions are denoted respectively ξ_A and ξ_B , its Gibbs energy then reads:

$$G^L = \xi_A G_A + \xi_B G_B + RT (\xi_A \ln \xi_A + \xi_B \ln \xi_B) \quad (2)$$

Rewriting equation (2) by introducing the Gibbs energy difference $\Delta G^d = G_B - G_A$ between the 2 states and only keeping $\xi = \xi_B$ gives:

$$G^L = G_A + \xi \Delta G^d + RT ((1 - \xi) \ln (1 - \xi) + \xi \ln \xi) \quad (3)$$

In a true binary ideal solution, ξ is an external variable that can be controlled by the experimentalist while in equation (3), ξ value adjusts itself to the temperature changes. The equilibrium value of ξ is hence obtained at each temperature by the condition of minimum Gibbs energy:

$$\frac{\partial G^L}{\partial \xi} = 0 \quad (4)$$

An explicit, single-value function of temperature, of the B molar fraction at equilibrium, here denoted ξ_e , is obtained:

$$\xi_e = \frac{\exp\left(-\frac{\Delta G^d}{RT}\right)}{1 + \exp\left(-\frac{\Delta G^d}{RT}\right)} \quad (5)$$

Two alternative and useful forms of the internal equilibrium condition are:

$$1 - \xi_e = \frac{1}{1 + \exp\left(-\frac{\Delta G^d}{RT}\right)} \quad (6)$$

$$\Delta G^d = -RT \ln \frac{\xi_e}{1 - \xi_e} \quad (7)$$

These equations have been derived many times and can also be found in some classic textbooks [4] pages 297-299. The model defined according to equations (2) to (5) will be named in the following the “ideal 2-state model”.

Following Agren's pioneering work [11], most CALPHAD researchers have adopted this model for describing the liquid with an increasing number of articles focused on the description of pure elements, mainly metallic, in the context of the development of 3rd generation databases e.g. [25] [26] [14] [27] [28] [29] and also including few binaries e.g. [30] [31]. This list is not exhaustive as new works are regularly published.

It is now interesting to question the nature of the two types of structural entities A and B composing the liquid. According to Agren [11], they correspond to localized (A) vs. non-localized (B) atoms or molecules. Borrowing a terminology coming from the free-volume theory of the glass transition [32] [33], these two types were later qualified as solid-like (A), having only vibrational degrees of freedom, vs. liquid-like (B), having translational degrees of freedom, atoms or molecules [12]. Note that the term liquid-like is somewhat misleading if, following Frenkel¹ [34] and Trachenko and Brazhkin [35], it is considered that particle dynamics in the liquid state “can be separated into solid-like oscillatory and gas-like diffusive components”. Hence the term “gas-like” for B entities could possibly be more appropriate. The state A is assimilated to an “ideal amorphous solid” [11] in which defects are gradually incorporated as temperature is increased.

Very few practitioners of the CALPHAD method have applied the 2-state model to oxides, an example being the very recent description of the Ca-O system by Deffrennes et al. [36] but, to our knowledge, the first study in this category was due to Golczewski et al. [37]. This work is original by several aspects. First, the authors propose an interesting methodology for estimating the thermodynamic properties of the simple oxides Al₂O₃, CaO, MgO in their hypothetical ideal amorphous state on the basis of the existing data on vitreous silica and three vitreous silicates Wollastonite, Diopside and Anorthite. Second, they use a 2-state model having the analytical form:

$$G^L = G_A + \xi \Delta G^d + RT \left((1 - \xi) \ln (1 - \xi) + \xi \ln \xi \right) + G^{XS} \quad (8)$$

In equation (8), ξ is said to represent a fraction of “structural fluctuation” between the two states and the excess term is written as a sub-regular Redlich-Kister expansion having two terms:

$$G^{XS} = \xi(1 - \xi) (L_0 + L_1(1 - 2\xi)) \quad (9)$$

The introduction of the excess term in the 2-state model has several consequences. Depending on the complexity of the excess term, equation (4) may not have an analytical solution and the equilibrium value of ξ has in this case to be found numerically. Moreover, this equation may also have several solutions hence yielding several ξ_e values. This can be easily understood if, for example, $L_1 = 0$ in equation (9) and the excess term reduces to a constant positive interaction parameter L_0 . The 2-state model becomes in this case formally equivalent to a binary solution with a demixing tendency. On cooling, at temperatures

¹ Page 98: “...those continuous variations of different properties of liquids which take place with increase of volume and temperature, and which gradually shift the liquid state from the solid-like to the gas-like type.”

lower than a critical value, demixing will be predicted between two co-existing liquids having the same composition, one being solid-like rich while the other is liquid-like rich. Such a variation of the model has been applied to the description of liquid silicon by Stolen and Grande [38] (pages 143-149). In this last case, demixing in a unary liquid is said to be energy driven.

Holten and Anisimov [39] have modeled liquid-liquid separation in supercooled water using another variant of the 2-state model. They consider that pure liquid water is a mixture of two states of structures A, corresponding to a High-Density Liquid (HDL), and B corresponding to a Low-Density Liquid (LDL). They assume that the solution is athermal, hence having a zero-mixing enthalpy, but exhibiting an excess entropy. The Gibbs energy of the liquid then reads:

$$G^L = G_A + \xi \Delta G^d + RT \left((1 - \xi) \ln(1 - \xi) + \xi \ln \xi + \omega \xi(1 - \xi) \right) \quad (10)$$

In which $\omega = \omega(p)$ depends on pressure p but not on temperature. Liquid-liquid separation is said to be entropy driven in this case.

Considering melts of semi-conductors as being essentially metallic liquids containing an equilibrium concentration of clusters with covalent bonds, Ponyatovski and Barkalov [40] have written the Gibbs energy of the liquid as a pseudo-binary regular solution:

$$G^L = \xi_A(E_A - TS_A) + \xi_B(E_B - TS_B) + \xi_A \xi_B E_{mix} + RT \left(\xi_A \ln(\xi_A) + \xi_B \ln(\xi_B) \right) + p(\xi_A V_A + \xi_B V_B) \quad (11)$$

Where ξ_A, E_A, S_A, V_A and ξ_B, E_B, S_B, V_B are the concentrations, energies, entropies and volumes of the ground (A) and excited (B) states respectively, E_{mix} being the mixing energy.

Finally, to describe any liquid, a general 2-state model was proposed by Tanaka [41] under the form:

$$G^L = \xi_A E_A + \xi_B E_B + (\xi_A V_A + \xi_B V_B)p + RT \left(\xi_A \ln(\xi_A/g_A) + \xi_B \ln(\xi_B/g_B) \right) + J \xi_A \xi_B \quad (12)$$

In this model, the liquid is composed of a mixture of normal-structures (A) and locally favored structures (B) representing the medium-range order. E_i, V_i, g_i are respectively the internal energy, the volume and the degeneracy of the state i and the energetic interaction parameter $J > 0$ because of frustration effect. Taking $S_i = R \ln g_i$ in equation (11) renders this equation formally equivalent to equation (12).

This short overview shows few variants of the 2-state model which are more complex than the ideal 2-state model generally used in most of CALPHAD works. These variants can be of interest depending on the specific liquid to be described. For example, it is likely that the ideal solution entropy is no longer appropriate for a liquid in which the entities that form the mixture have very different sizes.

In the next subsection, the ideal 2-state model is further analyzed.

1.2 Analysis of the ideal 2-state model

A detailed presentation of the model can already be found in various literature references such as [12] or [13] and [4] (pages 297-299), however, for the sake of completeness, we found relevant to start our analysis by recalling some important equations.

If the solid-like and liquid-like entities are denoted respectively using the superscripts "sol" and "liq", ξ being the fraction of liquid-like entities, which could alternatively be named using the Schmelzer and Gutzow [8] terminology the "structural order parameter" of the liquid, then:

$$G^L = G^{sol} + \xi \Delta G^d + RT(\xi \ln \xi + (1 - \xi) \ln(1 - \xi)) \quad (13)$$

At equilibrium, injecting the ξ_e expression (5) and rearranging:

$$G^L = G^{sol} - RT \ln(1 + \exp(-\Delta G^d/RT)) \quad (14)$$

Using the classical thermodynamic relations $G^i = H^i - TS^i$ and $C_p^i = \partial H^i / \partial T$ and again using expression (5), it can also be shown that:

$$S^L = -\frac{\partial G^L}{\partial T} = S^{sol} + \xi_e \Delta S^d - R(\xi_e \ln \xi_e + (1 - \xi_e) \ln(1 - \xi_e)) \quad (15)$$

$$H^L = H^{sol} + \xi_e \Delta H^d \quad (16)$$

$$C_p^L = C_p^{sol} + \xi_e C_p^d + \frac{d\xi_e}{dT} \Delta H^d \quad (17)$$

The configurational heat capacity of the liquid at equilibrium then reads:

$$C_p^{conf} = C_p^L - C_p^{sol} = \xi_e C_p^d + \frac{d\xi_e}{dT} \Delta H^d \quad (18)$$

To calculate the heat capacity of the liquid at equilibrium using equations (17) or (18), the derivative of the internal variable with respect to temperature must first be evaluated. By deriving expression (5), we find:

$$\frac{d\xi_e}{dT} = \frac{\Delta H^d}{RT^2} \frac{\exp(-\Delta G^d/RT)}{(1 + \exp(-\Delta G^d/RT))^2} \quad (19)$$

As $\Delta H^d > 0$, $d\xi_e/dT > 0$ and $\xi_e(T)$ is a monotonically increasing function from 0 to 1 with T .

All the above equations are independent of the analytical form chosen for ΔG^d . It is also worth noting that if equation (13) is of general validity, all other equations only hold true at equilibrium because equation (5) was used in their derivation. To indicate this, we have kept the subscript "e" for ξ in these equations.

It is our belief that the physical interpretation of the ideal 2-state model needs some clarification and we now want to emphasize that, when used alone, it is by construction unable to model the glass transition phenomenon observed in typical glass forming liquids. We will invoke two arguments.

First, the model implemented using equation (5) and (14) to (19) necessarily depicts a stable or, for $T < T_m$ (T_m being the melting temperature) metastable, liquid in internal equilibrium. Whatever the temperature, the internal variable ξ is not frozen-in. Being an equilibrium phase, the "sol" phase should hence obey the 3rd law and have a zero entropy at 0 K as already recognized in [12] and widely adopted in the CALPHAD literature. It can be noted by the way that the "sol" phase is not a glass in the sense of the Kauzmann's definition quoted at the beginning of the present article. To assess the validity of the assimilation of the "sol" phase to the so-called "ideal amorphous solid" or "ideal glass" requires to come back to the definition of this concept which is still under debate. Condensing Turnbull's definition [42] "an ideal glass is a solid in internal equilibrium... which exhibits an infinite unit cell". According to Angell [43], the ideal glass represents "the ground state for amorphous packing". This state would only be reached if the liquid could be slowly cooled in equilibrium down to Kauzmann's iso-entropy temperature T_K . One way of avoiding the entropy crisis is then for the liquid to form an "ideal glass" of unique configuration through an underlying "ideal glass transition" at T_K [44]. However, the prediction of the Kauzmann's temperature relies on an extrapolation of the metastable liquid heat capacity at temperatures lower than the glass transition temperature T_g . Nemilov's, in his striking Figure 9 page 60 of [5], shows two possible extrapolations one giving rise to an entropy crisis and the other not. Such entropy crisis is not calculated with the 2-state model which, by construction, assumes no anomaly in the evolution of the thermodynamical functions. The entropy difference between the liquid and the crystal phases, also called the excess entropy of the liquid, is calculated to reduce gradually on cooling vanishing only at 0 K (e.g. dashed blue curve Figure 13) and not at a strictly positive Kauzmann's temperature. Hence, our view is that the "sol" phase is more likely to represent a metastable liquid at 0 K than an "ideal glass" or "ideal amorphous solid", disregarding the open question of the real existence of such a solid. For a much more advanced discussion of these issues, including the reformulated definition of the entropy crisis on the basis of a non-negative entropy criterion instead of the more classical iso-entropic one and the distinction between a metastable liquid and the "ideal glass" the reader is referred to the works of Gujrati et al. [45] [46].

Second, the large heat capacity hump, also called Schottky heat capacity anomaly, described by the simultaneous use of equations (5), (18) and (19) is very different from the sharp heat capacity drop which occurs in a narrow temperature range for glass forming liquids. To further elaborate on this point, it is necessary to choose an analytical expression for the Gibbs energy difference between the two states.

Adopting a classical CALPHAD expansion of ΔG^d :

$$\Delta G^d = A + BT + CT \ln T + DT^2 + \dots \quad (20)$$

in which for physical reasons $A > 0$ and $B < 0$, it is found that:

$$\Delta S^d = -B - C - C \ln T - 2DT + \dots \quad (21)$$

$$\Delta H^d = A - CT - DT^2 + \dots \quad (22)$$

$$C_p^d = -C - 2DT + \dots \quad (23)$$

Keeping only the three first terms in equation (20), the configurational heat capacity is plotted vs. temperature in Figure 1a) and b) for various values of the A , B and C parameters. Increasing the A value, e.g. from 5000 to 20000 $J mol^{-1}$, shifts the summit of the peak towards higher temperatures but also considerably enlarges the peak width. Adding an entropic contribution, here a value corresponding to the communal entropy (for definition of this concept cf. pages 290-291 of ref. [47]) $B = -R$ was chosen, increases the peak height. The C coefficient represents a heat capacity difference between the solid-like and liquid-like states. It is seen that adding a non-zero C value, e.g. $C = -1 J mol^{-1} K^{-1}$, offsets the high temperature limit of the configurational heat capacity limit from 0 to $-C$ simultaneously increasing the peak height.

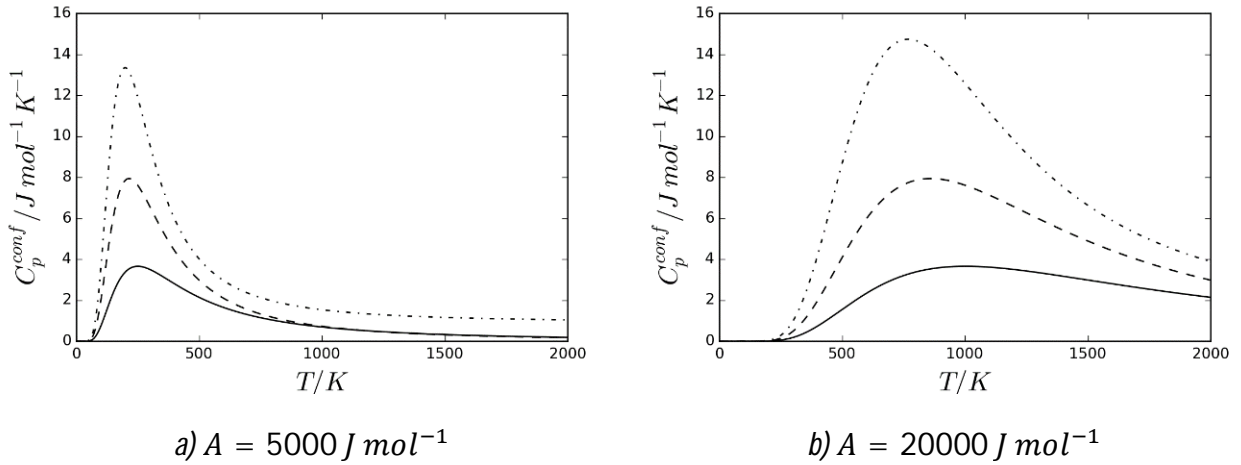


Figure 1. Configurational heat capacity of the liquid at equilibrium vs. temperature for $\Delta G^d = A + BT + CT \ln T$ and two different A values. Solid lines $B = C = 0$, dashed lines $B = -R, C = 0$, dash-dotted lines $B = -R, C = -1 J mol^{-1} K^{-1}$.

Figure 1 shows that the heat capacity anomaly, even when A has a small value e.g. 5 $kJ mol^{-1}$, spreads over several hundreds of K, drastically differing from the heat capacity evolution which is effectively recorded vs. temperature in a typical DSC experiment performed through the transition range of a glass forming substance.

It is proposed in [36] to roughly estimate for CaO “the glass transition temperature at the half of the heat capacity increase”. If the validity of this assertion is difficult to assess in the case of CaO which is hardly obtained as a glass and can only possibly undergo an “ideal glass transition”, for a typical glass forming substance such as B_2O_3 , the glass transition temperature has no direct connection with the heat capacity increase predicted by the equilibrium 2-state model as will be shown by the graphical representation of Figure 12c. Moreover, it is obvious that such an equilibrium model cannot simulate the hysteresis loops of the heat capacity and other quantities in the glass transition range.

It is now interesting to derive analytical expressions of the thermodynamic functions of general validity holding true both under equilibrium and non-equilibrium conditions.

By direct derivation of equation (13) with respect to temperature, without using equation (5), the entropy reads:

$$S^L = S^{sol} + \xi \Delta S^d - R(\xi \ln \xi + (1 - \xi) \ln(1 - \xi)) - \frac{d\xi}{dT} \left\{ \Delta G^d + RT \ln \frac{\xi}{1 - \xi} \right\} \quad (24)$$

At equilibrium, due to equation (7), the expression between braces in the third term cancels out and equation (15) is recovered.

At the glass state, ξ is frozen-in and hence no longer dependent on temperature. The third term cancels out and equation (15) is again recovered but this time because $d\xi/dT = 0$.

It is thus established that equation (15) holds true both in the equilibrium liquid and in the glass state.

Combining equations (13) and (24), the enthalpy in the glass transition range reads:

$$H^L = G^L + TS^L = H^{sol} + \xi \Delta H^d - T \frac{d\xi}{dT} \left\{ \Delta G^d + RT \ln \frac{\xi}{1 - \xi} \right\} \quad (25)$$

Similarly, the third term cancels out for both the equilibrium liquid and the glass state giving again equation (16).

By derivation of the enthalpy expression (25) with respect to temperature and after some grouping of terms, the heat capacity expression is also found:

$$C_p^L = C_p^{sol} + \xi C_p^d + \frac{d\xi}{dT} \Delta H^d - \frac{d\xi}{dT} \left\{ \Delta G^d + T \frac{d\Delta G^d}{dT} + 2RT \ln \frac{\xi}{1 - \xi} + \frac{RT^2}{\xi(1 - \xi)} \frac{d\xi}{dT} \right\} - T \frac{d^2\xi}{dT^2} \left\{ \Delta G^d + RT \ln \frac{\xi}{1 - \xi} \right\} \quad (26)$$

The expression between braces which is multiplied by $d\xi/dT$ cancels out at equilibrium because equation (7) implies that the sum of its first three terms equals $-\Delta H^d$, while, combining equations (5) (6) and (19), it can be shown that the fourth term equals ΔH^d , so the whole expression cancels out. Moreover, the expression between braces which is multiplied by $d^2\xi/dT^2$ obviously cancels out at equilibrium because of equation (5). Hence, at equilibrium, equation (26) reduces to its first three terms and the equilibrium heat capacity equation (17) is recovered.

At the glass state, the first and second derivatives of the structural order parameter with respect to temperature cancel out and the heat capacity equation (26) reduces to its first two terms.

1.3 Models of the crystal and liquid/glass phases

We have chosen to describe the vibrational part of the heat capacity of the various phases using weighed sums of Einstein functions. It was demonstrated by Voronin et al. [48] [49] [50] that this method is very efficient for fitting thermodynamic properties of oxides over a wide temperature range. This method was also adopted in the recent description of CaO by Deffrennes et al. [36]. In the present work, it proved to be well suited to fit the experimental heat capacity data of crystalline and glassy B_2O_3 .

The heat capacity is written under the form:

$$C_p(T) = \sum_i 3R\alpha_i \left(\frac{\Theta_i}{T} \right)^2 \frac{e^{\Theta_i/T}}{(e^{\Theta_i/T} - 1)^2} \quad (27)$$

The high temperature limit of the heat capacity hence reads:

$$C_p(\infty)/J\ mol\ at^{-1}K^{-1} = 3R \sum_i \alpha_i \quad (28)$$

By integrating $C_p d\ln T$ and taking the integration constant equals to 0 because it is assumed that both the crystal and the “sol” phase obey the 3rd law, the entropy is obtained:

$$S(T) = \sum_i 3R\alpha_i \left(\frac{\Theta_i}{T} \frac{e^{\Theta_i/T}}{e^{\Theta_i/T} - 1} - \ln(e^{\Theta_i/T} - 1) \right) \quad (29)$$

By integrating $C_p dT$ and taking the integration constant equals to the enthalpy value at 0 K $H(0)$, the enthalpy reads:

$$H(T) - H(0) = \sum_i \alpha_i \frac{3R\Theta_i}{e^{\Theta_i/T} - 1} \quad (30)$$

In 3rd generation descriptions of non-glass forming substances, and because of the lack of experimental data on the “sol” phase, the Gibbs energy difference between the crystal and the “sol” phase is usually taken as [12] [13]:

$$G^{sol} = G^{cryst} + A' \quad (31)$$

Equation (31) implies that the crystalline and “sol” phases have the same heat capacity and that their Gibbs energies only differ by a constant enthalpy value A' to be adjusted in the course of the optimization.

Contrarily, for a glass former, the availability of heat capacity data for the glass phase allows to model the heat capacities of the crystal and the “sol” phase using two different sets of (α_i, Θ_i) parameters in equation (27). Moreover, the enthalpy of the isothermal reaction:



Can be indirectly measured by performing solution calorimetry experiments on both the crystal and the glass using a well-chosen solvent and temperature, usually 298.15 K if both phases can be dissolved in an aqueous solution. Hence, this information can be used to adjust the enthalpy difference between the crystal and the “sol” phase, even if, for a real glass this enthalpy difference depends on the condition of preparation of the glass: the higher the fictive temperature of the glass, the larger the enthalpy difference. A concise definition of the concept of fictive temperature introduced by Tool [51] [52] is given by Goldstein [53] under the form: “the temperature at which the configurational state of the glass would be an equilibrium state of the liquid”.

Finally, the liquid phase will be described using the ideal 2-state model already presented in subsections 1.1 and 1.2.

For the numerical application in the case study of B_2O_3 , the (α_i, Θ_i) vectors of the crystal and amorphous phase were optimized using the freely available CpFit program [49]. Parameters $(A, B, C, D$ in equation (20)) of the Gibbs energy difference between the solid- and liquid-like states were optimized by a non-linear least square method using a homemade program written in Python based on the *lmfit* package. Graphs are generated with the *matplotlib* graphical library.

1.4 Review of experimental thermodynamic data of B_2O_3

Various recent CALPHAD descriptions of B_2O_3 are available in the literature [54] [55] [56] [57]. However, all are based on 1-state approaches for the liquid phase and hence not suitable for coupling with a relaxation law. The study of Decterov et al. [54] is the only one in which the glass transition is taken into account, modeling the transition by a sharp variation of the heat capacity of the liquid/amorphous phase in the 484-557 K range. Hence a new description, employing the 2-state model for the liquid phase, is required.

Experimental data on the thermodynamic functions of B_2O_3 are now reviewed starting with the heat capacity.

The crystal heat capacity was measured by adiabatic calorimetry by Kelley [58] between 53 and 295 K, Kerr et al. [59] between 18 and 297 K and Shmidt [60] from 304 K up to the melting point. The three datasets are in very good agreement as can be seen in Figure 2. The enthalpy increment was measured by drop calorimetry by Southard [61].

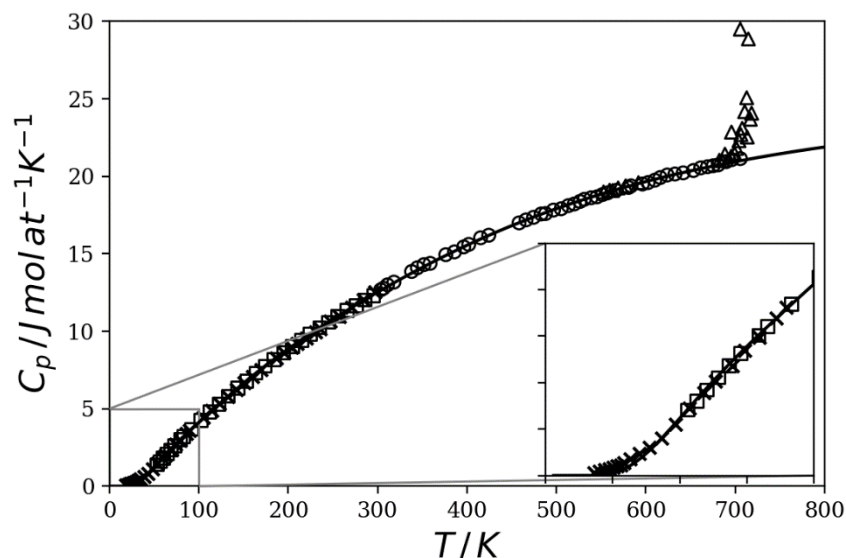


Figure 2. Heat capacity of crystalline B_2O_3 measured by adiabatic calorimetry, (\square) Kelley [58], (\times) Kerr et al. [59], (\circ) Shmidt [60], (Δ) pre-melting region Shmidt [60] compared with the modeling from this work (solid line)

The heat capacity of the glass and the liquid was measured by adiabatic calorimetry by Turdakin and Tarasov [62] between 60 and 295 K, Richet et al. [63] between 5 and 334 K and Shmidt [60] from 307 to 911 K and by Thomas and Parks [64] on heating and cooling between 307 and 618 K using a radiation scanning calorimeter and Moynihan et al. [65] on heating between 400 and 682 K by DSC. The results of Moynihan et al. are only presented graphically in the original article so the experimental values were obtained by digitizing figures 3 and 5 of the article with the help of the free Plotdigitizer² software, with the inherent uncertainty linked to such procedure.

All the data are compared in Figure 3 showing an overall good agreement between various authors with the notable exception of the pioneering results obtained by Thomas and Parks [64] in the glass transition range (blue and red points in Figure 3). While the results of Moynihan et al. [65] obtained with a commercial DSC in 1976 smoothly join the adiabatic calorimetry results on both sides of the glass transition, the values of Thomas and Parks are systematically shifted to lower values, particularly on the liquid side of the transition. It is likely that these values are underestimated because of an erroneous evaluation of the calibration coefficient of their radiation calorimeter. Thomas and Parks have assessed the absolute error of their measurements to be lower than 4%. This was a very accurate estimation considering that on the liquid side, their value is approximately 4.5% lower than the adiabatic measurements obtained by Shmidt 35 years later. However, another drawback of Thomas and Parks study is that the thermal conditions of the experiments are only loosely specified using expressions such as “on heating after very fast cooling”, “on cooling from the liquid” and “on heating after slow cooling”. It can also be observed that, according to Thomas and Parks, and despite “very fast cooling” in one of the runs, the glass transition occurs at lower temperatures than shown by Moynihan et al. results obtained using moderate cooling rates, and by the Shmidt study, both being in agreement. So, the possibility of a temperature calibration error cannot be totally excluded. As a conclusion, the three datasets of Thomas and Parks were discarded.

² <http://plotdigitizer.sourceforge.net/>

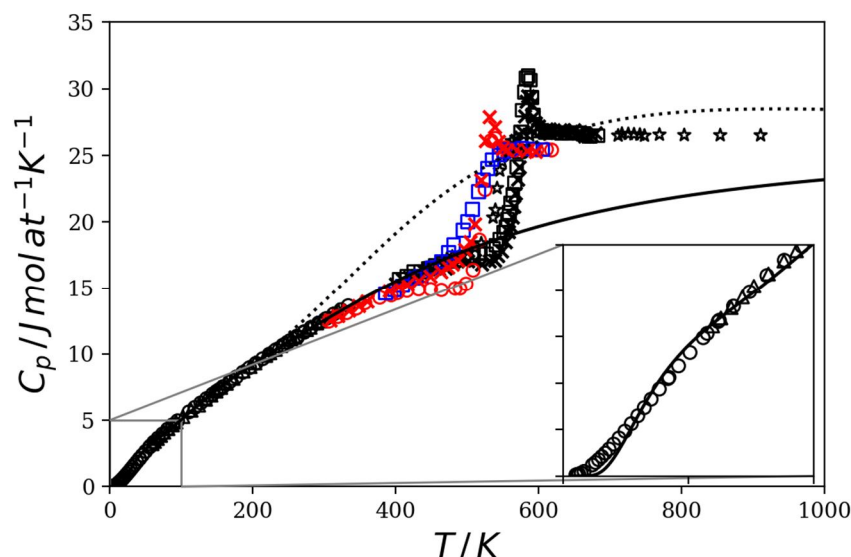


Figure 3. Heat capacity of B_2O_3 at the glass and liquid states. Adiabatic calorimetry: black (Δ) Turdakin and Tarasov [62], black (\circ) Richet et al. [63], black (\star) Shmidt [60]. Radiation scanning calorimetry: red (\circ) on heating after very fast cooling, blue (\square) on cooling from the liquid, red (\times) on heating after slow cooling, Thomas and Parks [64]. DSC: black (\square) on heating at 10 K min^{-1} after prior cooling at -10 K min^{-1} , black (\times) on heating at 10 K min^{-1} after prior cooling at -80 K min^{-1} Moynihan et al. [65]. Modeling from this work, solid-like state (solid line), liquid (dotted line).

The enthalpy increment $H^L(T) - H^L(298)$ of the glass/liquid was measured by drop (from high temperature to room temperature) calorimetry by Southard [61] between 382 and 1777 K, Krasovitskaya et al. [66] between 1015 and 2154 K, Shpil'Rain et al. [67] between 766 and 2211 K and by transposed (from room temperature to high temperature) drop calorimetry by Klein and Müller [68] at 1725 and 1775 K. All the data are in good agreement as shown in Figure 4 except the two measuring points of Klein and Müller which lie outside the experimental scattering of the values from the other studies, probably because these last authors used a calorimetric technique which does not allow the sample to be encapsulated and could vaporize, as already pointed out by Decterov et al. [54].

The main source of systematic error in the three studies having used drop calorimetry is the ill-defined glass state of the sample at room temperature. It is likely that the samples quenched from very high temperatures (e.g. $T > 2000\text{ K}$) undergo a higher cooling rate and hence would reach a glass state of higher enthalpy than the ones quenched from moderate temperatures (e.g. $T < 1000\text{ K}$). This effect may possibly lead to an underestimation of the heat increment.

Discarding the two datapoints of Klein and Müller, all the results in the liquid at $T > 610\text{ K}$ can be fitted to a straight line (black dotted line in Figure 4) having a slope equal to $25.611 \pm 0.064\text{ J mol}^{-1}\text{ K}^{-1}$. Trying to fit the data with a quadratic polynomial showed that the coefficient of the quadratic term was statistically meaningless. Hence, it can be concluded from the three drop calorimetry studies that the liquid exhibits a constant heat capacity over the 610-2154 K range.

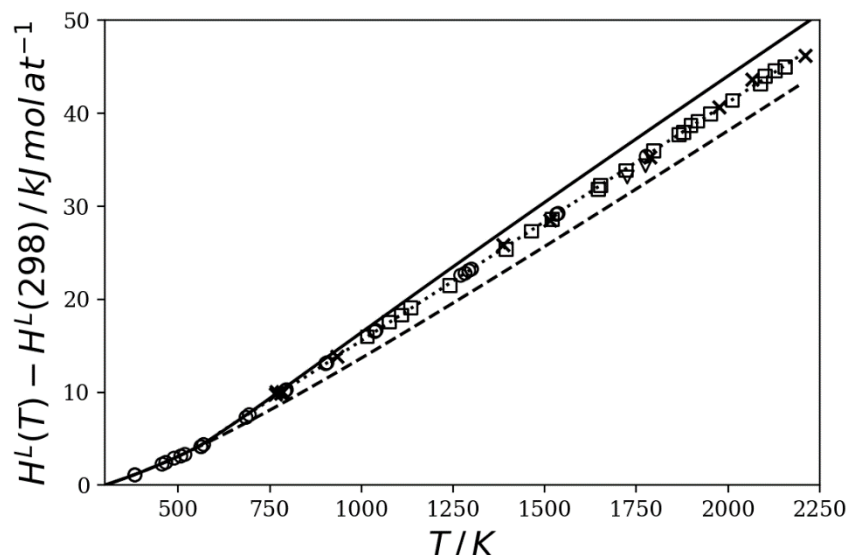


Figure 4. Heat increment of B_2O_3 at the glass and liquid states. Drop calorimetry: (\circ) Southard [61], (\square) Krasovitskaya et al. [66], (\times) Shpil'Rain et al. [67] and linear regression to the data with slope $25.611 \pm 0.064 \text{ J mol at}^{-1} \text{ K}^{-1}$ (dotted line). Transposed drop calorimetry (∇) Klein and Müller [68]. Modeling from this work using the A and B parameters given in Table 6 for the solid-like (dashed line) and liquid (solid line) states.

The internal discrepancy between the selected heat capacity data and the heat increment of the liquid phase is emphasized in Figure 5. The direct measurements of the heat capacity (empty circles) by adiabatic scanning calorimetry lie in the range $26.5 - 27 \text{ J mol at}^{-1} \text{ K}^{-1}$ while a constant $25.611 \pm 0.064 \text{ J mol at}^{-1} \text{ K}^{-1}$ value (black dashed line) is inferred from the heat increment data obtained by drop calorimetry. Decterov et al. [54] chose to discard the heat capacity adiabatic measurements of Schmidt [60] in favor of a constant $25.556 \text{ J mol at}^{-1} \text{ K}^{-1}$ heat capacity value (red dotted line) on the basis of drop calorimetry data. This description was also recently adopted by Utlak and Besmann [57]. Estimating a large $\pm 2.5 \text{ J mol at}^{-1} \text{ K}^{-1}$ uncertainty on the measured values by both techniques, an intermediate $25.9408 \text{ J mol at}^{-1} \text{ K}^{-1}$ constant value (red dashed line) is selected as a compromise in the JANAF tables [69]. Interestingly, a different compromise is found in CODATA [70] and Gurvich et al. [71] tables in which the liquid heat capacity (red dash-dotted curve) decreases from the adiabatic values above the melting point down to the drop calorimetry value above 2000 K.

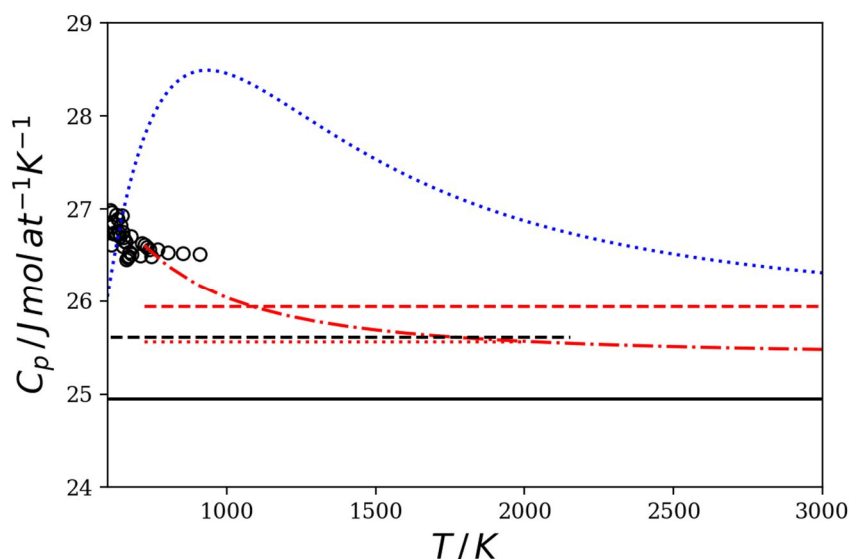


Figure 5. Heat capacity of equilibrium B_2O_3 liquid. Horizontal solid line = $3R$ Dulong-Petit limit. (\circ) selected measurements from Schmidt [60] by adiabatic calorimetry or Moynihan et al. [65] by DSC. Black dashed line, constant $25.611 \pm 0.064 \text{ J mol at}^{-1} \text{ K}^{-1}$ heat capacity from linear regression to heat increment measurements. Red

dash-dotted curve, CODATA [70] and Gurvich et al. [71] recommended curve. Red dashed line, JANAF [69]. Red dotted line, Decterov et al. [54]. Blue dotted line, modeling from this work.

Thermodynamic data of the crystal and the liquid/glass phases from various reference compilations are compared in Table 1 to the data selected or optimized in the present work.

The standard formation enthalpy of the crystal at 298.15 K, $\Delta_f H_{298}^{cryst}$, was critically assessed in both the JANAF tables [69] and the CODATA key-values [70]. The two assessed values, $-1271.9 \pm 2.1 \text{ kJ mol}^{-1}$ and $-1273.5 \pm 1.4 \text{ kJ mol}^{-1}$ respectively, agree considering the uncertainties. The CODATA recommended value, based on the simultaneous least square evaluation of the formation enthalpies of B_2O_3 , H_3BO_3 and BF_3 and relying on a large number of reaction enthalpy measurements, is adopted in the tables of Gurvich et al. [71] and in this work.

The vitrification enthalpy corresponding to reaction (32) was measured by water solution calorimetry by Johnson and Hubbard [72]: $\Delta_{vitr} H_{298}^\circ = 18.577 \pm 0.251 \text{ kJ mol}^{-1}$. From this value and the standard formation enthalpy of the crystal, the standard formation enthalpy of the glass can be derived.

The melting temperature $T_m = 723 \text{ K}$ is adopted by JANAF, CODATA and Gurvich et al. The uncertainty $\pm 1 \text{ K}$ assessed by Gurvich et al. is also selected in this work.

The melting enthalpy selected in JANAF tables is $\Delta_m H_{723} = 24.071 \pm 0.4 \text{ kJ mol}^{-1}$, this value being indirectly evaluated by combining the vitrification enthalpy at 298 K of reference [72] and the enthalpy increments of the crystal and liquid phases to extrapolate this enthalpy difference to the melting point. A slightly differing value $\Delta_m H_{723} = 24.56 \text{ kJ mol}^{-1}$ was adopted by CODATA without stating the uncertainty. This value corresponds to the direct measurement performed by Shmidt et al. [60] by adiabatic calorimetry: $\Delta_m H_{723} = 24.560 \pm 0.126 \text{ kJ mol}^{-1}$. The same last value is selected by Gurvich et al. but with a larger and more realistic uncertainty of $\pm 0.15 \text{ kJ mol}^{-1}$ which is also adopted in this work.

Table 1. Thermodynamic properties of B_2O_3 from JANAF [69], CODATA [70] and Gurvich et al. [71] tables compared to the values adopted in this work.

	JANAF	CODATA	Gurvich et al.	This work
$\Delta_f H_{298}^{cryst} / \text{kJ mol}^{-1}$	-1271.9 ± 2.1	-1273.5 ± 1.4	-1273.5 ± 1.4	-1273.5 ± 1.4
T_m / K	723 ± 0.5	723	723 ± 1	723 ± 1
$\Delta_m H_{723} / \text{kJ mol}^{-1}$	24.071 ± 0.4	24.560	24.56 ± 0.15	24.56 ± 0.15
$H^{cryst}(298) - H^{cryst}(0) / \text{kJ mol}^{-1}$	9.293	9.301 ± 0.040	9.301 ± 0.040	9.308
$H^{glass}(298) - H^{glass}(0) / \text{kJ mol}^{-1}$	10.060	No data	10.3 ± 0.1	10.185
$S^{cryst}(298) / \text{J mol}^{-1} \text{K}^{-1}$	53.95 ± 0.4	53.97 ± 0.30	53.97 ± 0.30	53.616
$S^{glass}(298) - S^{glass}(0) / \text{J mol}^{-1} \text{K}^{-1}$	61.826	No data	72.6 ± 1.6	66.141
$\Delta_{vitr} H_{298}^\circ / \text{kJ mol}^{-1}$	18.577 ± 0.251	No data	18.6 ± 0.3	18.577 ± 0.251
$\Delta_{vitr} H_0^\circ / \text{kJ mol}^{-1}$				17.7

The residual entropy of the glass $S^{glass}(0 \text{ K})$ at 0 K was estimated by various authors. The values are compared in Table 2.

Table 2. Residual entropy $S^{glass}(0 \text{ K})$ of B_2O_3 glass at 0 K having a fictive temperature T_f .

Reference	T_f / K	$S^{glass}(0 \text{ K}) / \text{J mol}^{-1} \text{K}^{-1}$
JANAF [69]	Not specified	16.617

Gurvich et al. [71]	Not specified	7.9 ± 1.0
Nemilov, Table 1, page 78 of reference [5]	540	11.09 – 11.38
Johari [73]	521	9.9
Richet et al. [63]	543	11.2 ± 0.8
Combined thermodynamic + kinetic modeling from this work, cooling at 1 K/min	540.77	12.2
Combined thermodynamic + kinetic modeling from this work, cooling at 0.025 K/min	520.06	11.1

The values from the JANAF and the Gurvich et al. tables seem to be less reliable than the other three because the transition temperature assumed for the glass is not specified.

Estimations from Richet et al. [63] and Nemilov [5] are in very close agreement around $11 \text{ J mol}^{-1} \text{ K}^{-1}$. Considering that the melting entropy of B_2O_3 that can be calculated from the selected values of the melting temperature and enthalpy (Table 1) is $\Delta_m S = 34 \text{ J mol}^{-1} \text{ K}^{-1}$, it can be noticed that these two estimations are in complete agreement with the Schmelzer and Gutzow's rule of thumb (equation 2.129 page 53 of reference [8]):

$$S^{\circ \text{glass}}(0 \text{ K}) \approx \frac{1}{3} \Delta_m S \quad (33)$$

Which is obeyed for a large number of glasses solidified at “normal” cooling rates.

A slightly lower value $10 \text{ J mol}^{-1} \text{ K}^{-1}$ is estimated by Johari [73] but assuming a lower fictive temperature (520 K) for the glass than in the studies of Nemilov and Richet et al. (540-543 K). Thus, the three estimations are likely to be consistent.

1.5 Results and discussion of the thermodynamic modeling

We started by fitting the thermal functions of the crystal and the “sol” phase.

For the crystal phase, the enthalpy increment dataset of Southard [61] was found to deviate from other data and degrade the quality of the modeling as already pointed out in the notes to the JANAF Tables. Considering that drop calorimetry is generally less accurate than adiabatic calorimetry and that the three adiabatic calorimetry datasets of Kelley [58] Kerr et al. [59] and Shmidt [60] are in remarkable agreement, the datapoints of Southard were finally excluded from the fitting procedure.

The number of Einstein functions was increased gradually until good agreement with the experimental data was achieved. For both the crystal and the amorphous solid, it was found that, from a purely statistical point of view, a sum of four Einstein functions (8 parameters) gave the optimal description. Increasing this number to five resulted in at least one statistically meaningless coefficient. Overfitting was hence avoided by keeping only four terms.

However, equation (28) implies that the high temperature limit of the vibrational contribution to the heat capacity increases with the number of Einstein functions. Using four Einstein functions for the crystal, it was found that the high temperature limit of the C_p was around ten percent above the Dulong-Petit C_V harmonic limit. Considering that the experimental heat capacity curves of the crystal and the glass merge above room temperature [63] indicating a similar high temperature behavior, such a high limiting value for the crystal, indeed higher than the heat capacity of the liquid phase itself, would possibly yield an unphysical negative configurational liquid heat capacity. On this basis, it was decided to keep only three Einstein terms in the sum, lowering the high temperature limit of the crystal heat capacity to 4% above $3R$.

The optimized coefficients of the thermodynamic model of the crystal phase are given in Table 3 and the calculated heat capacity curve is compared to the experimental data in Figure 2.

Table 3. Values of the weights and Einstein temperatures of the crystal phase optimized with the CpFit program on 117 experimental points obtained by merging the Kelley [58], Kerr et al. [59] and Shmidt [60] datasets. The Δ and s values are respectively the 95% confidence interval and standard deviations of the parameters. Non-significant digits are kept to avoid round-off errors.

i	α_i	$\Delta\alpha_i$	$s(\alpha_i)$	θ_i	$\Delta\theta_i$	$s(\theta_i)$
				/ K	/ K	/ K
1	0.465477187	0.0177244	0.00894466	1661.7511880	54.94200	27.72650
2	0.351207422	0.0156721	0.00790896	664.0531930	35.37290	17.85100
3	0.218574007	0.0139316	0.00703059	226.7094497	7.92836	4.00106

The experimental and calculated enthalpy increment of the crystal are compared in Figure 6. Despite the dataset of Southard not being taken into account in the optimization, the agreement is reasonable.

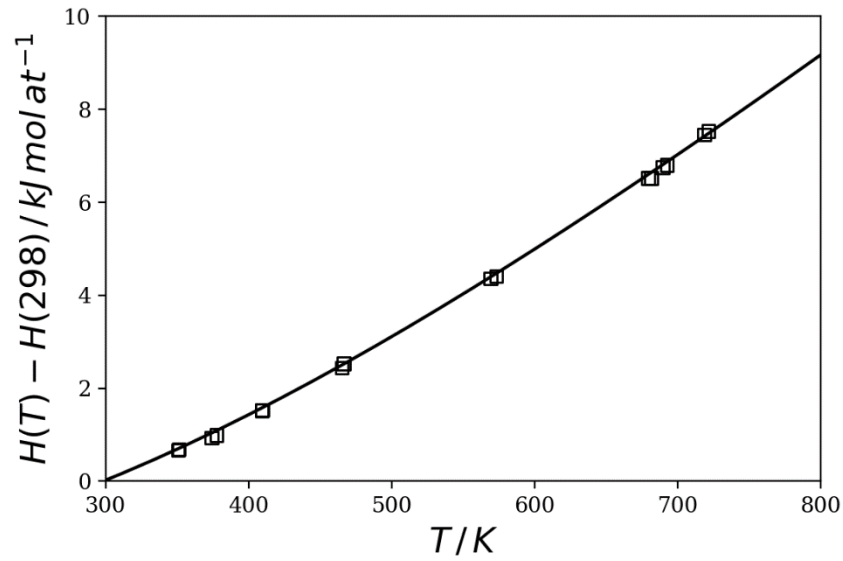


Figure 6. Enthalpy increment of crystalline B_2O_3 measured by drop calorimetry (\circ) by Southard [61] compared with the modeling from this work (solid line).

For optimizing the heat capacity parameters of the “sol” phase, and after having discarded the datasets of Thomas and Parks [64], we constructed a 108-point dataset by merging the datasets of Turdakin and Tarasov [62] and Richet et al. [63] and adding the experimental points of Shmidt [60] and Moynihan et al. [65] obtained at temperatures lower than the lower bound of the glass transition range. For the same reason as for the crystal phase, it was chosen to restrict the sum of Einstein functions to three terms. However, in this case, the high temperature limit of the heat capacity was found to only reach $0.95 \times 3R$ with a high temperature evolution becoming very different than the one of the crystal.

Finally, to constraint the heat capacities curves of the crystal and the “sol” phase to merge above room temperature, we added to the glass dataset 24 points measured by Shmidt [60] for the crystal in the temperature range comprised between the glass transition temperature and the melting point.

The resulting optimized coefficients of the heat capacity model of the glass are presented in Table 4 and the calculated heat capacity curve is compared to the experimental data in Figure 3.

Table 4. Values of the weights and Einstein temperatures of the glass optimized with the CpFit program on 132 experimental points obtained by merging the Turdakin and Tarasov [62] and Richet et al. [63] datasets, 8 datapoints at $T < 500$ K from Shmidt [60], 9 datapoints at $T < 440$ K from Moynihan et al. [65] and 24 crystal datapoints from Shmidt [60] in the range 526-706 K. The Δ and s values are respectively the 95% confidence interval and standard deviations of the parameters. Non-significant digits are kept to avoid round-off errors.

i	α_i	$\Delta\alpha_i$	$s(\alpha_i)$	θ_i	$\Delta\theta_i$	$s(\theta_i)$
				/ K	/ K	/ K
1	0.528162913	0.0135499	0.00684693	1600.727224	55.0723	27.8287
2	0.180141253	0.00822347	0.00415543	121.9903056	5.50505	2.78177
3	0.328836748	0.0157812	0.00797443	546.1879661	26.548	13.4151

The calculated heat capacity curves of the crystal and the glass are compared in Figure 7. It is seen that these two curves, which differ at low temperatures, actually merge close to room temperature well below temperatures at which the 3R Dulong-Petit limit would be approached. According to Richet et al. [63], “this indicates that the vibrational density of states consists of distinct low- and high- frequency range due to a soft medium-range organization”.

It can be checked from a close inspection of the insert of Figure 3, that the good high temperature behavior of the modeled heat capacity is obtained at the expense of a degradation of the prediction between 0 and 100 K. Such a compromise was judged acceptable in the present work.

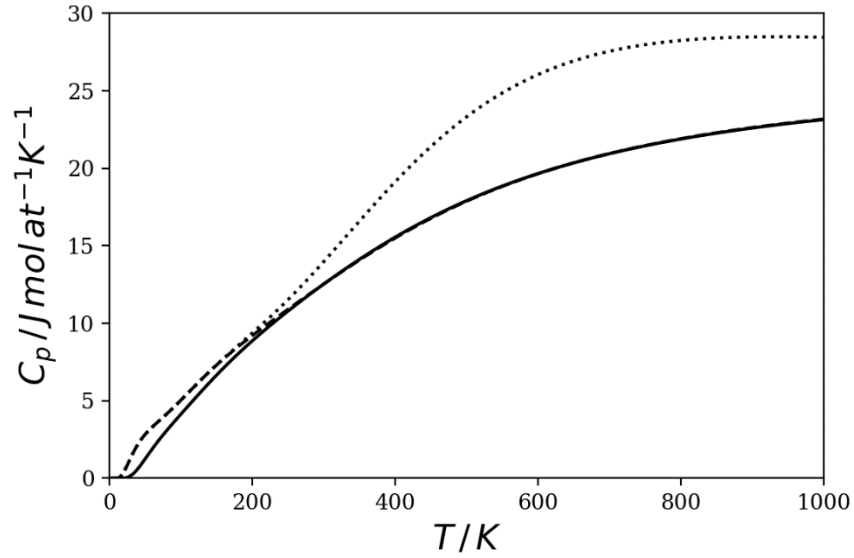


Figure 7. B_2O_3 heat capacity curves for the crystal (solid line), the “sol” phase (dashed line) and the equilibrium liquid (dotted line) phases calculated from this work with the coefficients given in Tables 3, 4 and 6.

The next step consists in adjusting the coefficients of the Gibbs energy differences between the solid- and liquid-like states (A, B, C coefficients... in equation 20) and between the “sol” phase and the crystal (A' in equation 31).

However, if the heat capacity of the glass at temperatures lower than the glass transition range can quite safely be assumed not to depend on the cooling conditions, it is not the case for other “thermodynamic” quantities characterizing the glass state such as the zero-point entropy $S^{\circ glass}(0\text{ K})$ and enthalpy $^{\circ glass}H_0 = \Delta_{vitr}H_0^{\circ} = H^{\circ glass}(0\text{ K}) - H^{\circ cryst}(0\text{ K})$ which are strongly dependent on both the cooling rate and values of the A, B, C coefficients.

A particular difficulty then arises from the fact that the validity of a given thermodynamic modeling cannot be assessed independently from the kinetic data and that the glass transition kinetics puts additional constraints on the thermodynamic optimization.

We expect the configurational part of the heat capacity to vanish at temperatures lower than the lower bound of the glass transition range which can be roughly estimated to be around 400 K on the basis of Figure 3:

$$C_p^L = C_p^{sol} \text{ for } T < 400\text{ K} \quad (34)$$

From equation 26, the heat capacity of the glass with frozen-in configuration also reads:

$$C_p^L = C_p^{sol} + \xi C_p^d \quad (35)$$

Considering that ξ has a non-zero value when it is frozen-in at the glass transition, equation (34) is fulfilled only if $C_p^d = 0$ in equation (35) or if using equation (23):

$$C = D = 0 \quad (36)$$

At this stage, it remains to adjust the coefficients A and B and the melting properties of the substance are particularly helpful for performing this task.

First, the entropy of the liquid in equilibrium at its melting point can be calculated using the heat capacity model of the crystal (Table 3) and the selected value of the melting enthalpy:

$$S^L(T_m) = \int_0^{T_m} \frac{C_p^{cryst}}{T} dT + \frac{\Delta_m H}{T_m} = 163.028 \text{ J mol}^{-1} \text{ K}^{-1} \quad (37)$$

Second, as already discussed in subsection 1.2, the “sol” phase is assumed to obey the 3rd law and its entropy at the melting point can be calculated using the optimized coefficients of the glass heat capacity model given in Table 4:

$$S^{sol}(T_m) = \int_0^{T_m} \frac{C_p^{glass}}{T} dT = 141.457 \text{ J mol}^{-1} \text{ K}^{-1} \quad (38)$$

The configurational entropy can thus be reliably estimated at the melting point combining equations (37) and (38):

$$S^{conf}(T_m) = S^L(T_m) - S^{sol}(T_m) = 21.570 \text{ J mol}^{-1} \text{ K}^{-1} \quad (39)$$

Because of equation (15), we also have:

$$S^{conf}(T_m) = \xi_e(T_m) \Delta S^d(T_m) - R(\xi_e(T_m) \ln \xi_e(T_m) + (1 - \xi_e(T_m)) \ln(1 - \xi_e(T_m))) \quad (40)$$

While $\Delta S^d(T_m)$ is only a function of B through equation (21), $\xi_e(T_m)$ is a function of both A and B through equations (5) and (20). Hence, because of equation (40), A and B cannot be adjusted independently in the optimization process.

We chose to set the value of B manually and then to compute the corresponding value of A by numerical solution of equation (40). Then the kinetic simulation was run and the quality of the optimization was judged from various thermodynamic and kinetic criteria as explained in subsection 2.4. The process was repeated by trial and error, changing the B value until an optimum value was found.

An alternative method was also attempted for automatic and simultaneous optimization of the A and B values. First a dataset was constructed by taking the 35 heat capacity experimental points (seen in Figure 5) of the liquid phase which have a temperature greater than 610 K, this temperature being the lower bound of the temperature range in which the liquid is in internal, whether it is stable or metastable, equilibrium. For each experimental point, the vibrational contribution was calculated using the $C_p(T)$ model of the “sol” phase and subtracted from the value in order to convert the C_p data to C_p^{conf} data. Then, the A and B parameters of the two-state model were adjusted using a least square Levenberg-Marquardt minimization algorithm. Despite the fact that heat capacity data could be very well fitted (Figure 8), this alternative method was not judged satisfactory because unrealistic too high values of the liquid entropy at the melting point and of the frozen-in entropy were obtained.

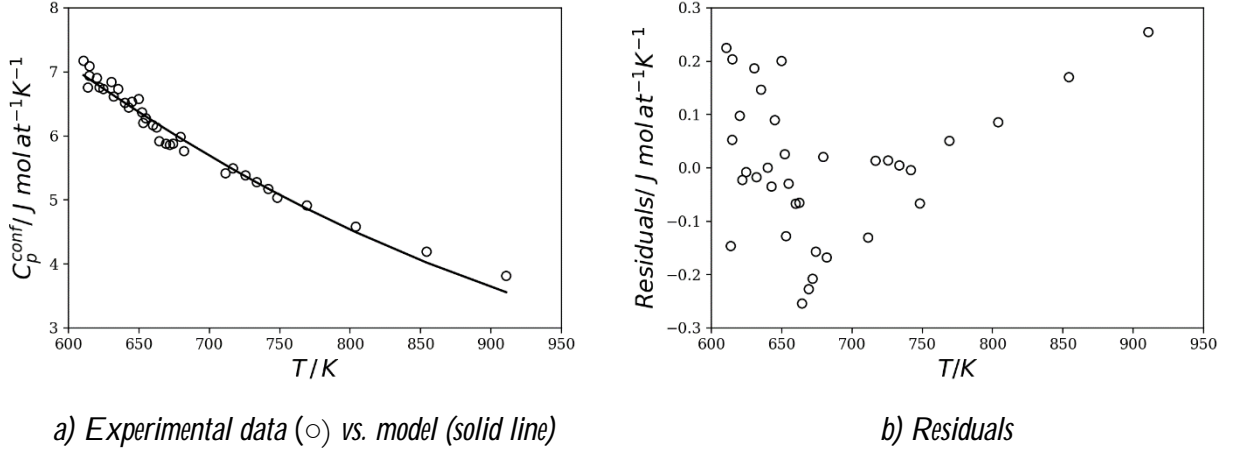


Figure 8. Optimization of A and B parameters by least square fit of the configurational heat capacity data of the liquid at $T > 610$ K. Optimized but not recommended (see text) values $A = 9919.46 \pm 85.04 \text{ J mol at}^{-1}$ and $B = -10.12050 \pm 0.36252 \text{ J mol at}^{-1} \text{ K}^{-1}$. Uncertainties on the coefficients are standard ones.

Finally, it must be emphasized that the value of the A' parameter in equation (31) cannot be optimized without using a kinetic model because this parameter represents the enthalpy difference between the “sol” phase and the crystal. Practically, such enthalpy difference can only be measured for a real, necessarily out of equilibrium, glass and in this case the measured value will be the sum of two contributions: a constant A' contribution and a variable frozen-in fraction of the melting enthalpy which depends on the cooling conditions.

2 Relaxation kinetics

2.1 Rate equation and relaxation laws

The reader interested by a comprehensive overview of relaxation phenomena in glasses is referred to the remarkable article of Hodge [74] and the reference monograph of Donth [75]. Only some key assumptions and equations useful for the present modeling are presented in this subsection.

By applying TIP, e.g. [76] or [8] pages 95-98, it can be shown that the rate of change of the internal variable can be written under the form:

$$\frac{d\xi}{dt} = -\frac{\xi - \xi_e}{\tau} \quad (41)$$

This ordinary differential equation describes the structural order parameter time relaxation towards its equilibrium value, τ being the characteristic relaxation time of the process. Alternatively, from a statistical physics approach based on the transition rates of a TLS model, a so-called Master Equation [19] having the same analytical form as (41) can be also derived.

However, time relaxation in glasses is non-exponential. The non-exponential character of the time response with which equilibrium is restored after a perturbation can mathematically be better represented by a distribution of relaxation times [77] [74] instead of a single one.

A simplifying approach to fit the data of relaxation experiments in the time domain consists in assuming an analytical form of the relaxation time distribution using a response function $\phi(t)$ having the so-called “stretched exponential” form, also known as Kohlrausch-William Watts decay function [77] [74]:

$$\phi(t) = \exp\left(-\frac{t}{\tau}\right)^\beta \quad (42)$$

In which $0 < \beta \leq 1$ represents the width of the distribution. The average relaxation time $\langle \tau \rangle$ is then

given by:

$$\langle \tau \rangle = \frac{\tau}{\beta} \Gamma\left(\frac{1}{\beta}\right) \quad (43)$$

Where Γ is the gamma function. The case $\beta = 1$, $\langle \tau \rangle = \tau$ corresponds to a process having a single relaxation time also called Debye relaxation.

In the particular case of B_2O_3 , the superior fitting ability of the stretched exponential form compared to other distribution functions, such as the log Gaussian and Cole-Davidson ones, was demonstrated by Moynihan et al. [78] (see also page 249 of [74]).

At this point, it is interesting to have a look on the various forms $\tau(T, \xi)$ which can be assumed for the dependency of the relaxation time on the thermodynamic external T and internal ξ variables.

Relaxation is thermally activated and hence a strong temperature dependence of the relaxation time is expected. In glasses, experimental plots of the logarithm of the relaxation time vs. reciprocal temperature show a curvature evidencing a non-Arrhenius behavior. One often used empirical form to fit the data is the Vogel- Fulcher-Tamman (VFT) equation:

$$\langle \tau \rangle = A_{VFT} \exp\left(\frac{B_{VFT} T_{VFT}}{T - T_{VFT}}\right) \quad (44)$$

In which A_{VFT} , B_{VFT} , T_{VFT} are temperature independent fitting parameters which have positive values and depend on the substance. The VFT equation is essentially an equilibrium relaxation law in the sense that the relaxation time only depends on temperature and is not affected by the internal state of the glass. By construction, such a law combined with the rate equation (41) is only able to describe a linear relaxation process. Hence complex non-linear relaxation observed in glasses cannot be properly described with this law.

The fact that the relaxation process also depends on the internal state of the glass can be intuitively understood: a glass having a high fictive temperature and a large fraction of free volume, would be expected to relax faster than a more compact one, having a correspondingly smaller fictive temperature.

A general functional form $\tau(T, \xi)$ of the relaxation time has been proposed by Gutzow et al. e.g. [76] [79] and applied to a hypothetical vitrifying substance having typical properties, in conjunction with a liquid lattice-hole model equally used to depict the dependency of the activation energy of the relaxation on the internal variable. To our knowledge, parametrization of this interesting non-linear relaxation model for a real glass is missing in the literature.

Other expressions of the relaxation time, more widely used in the glass research literature, are based on the Tool's fictive temperature concept [51] [52] to represent the internal state of the glass.

The first one is the so-called Tool-Narayanaswamy-Moynihan (TNM) relaxation law [80]:

$$\langle \tau \rangle = A_{TNM} \exp\left(\frac{x \Delta h^*}{RT} + \frac{(1-x) \Delta h^*}{RT_f}\right) \quad (45)$$

Where x is a mixing parameter ($0 \leq x \leq 1$), Δh^* the activation energy and T_f the fictive temperature. Equation (45) is sometimes called a modified Arrhenius equation [78]. Indeed, at equilibrium, the real temperature is equal to the fictive one, taking $T_f = T$ in equation (45) yields a simple Arrhenius function:

$$\langle \tau \rangle = A \exp\left(\frac{\Delta h^*}{RT}\right) \quad (46)$$

Depending on whether the heat capacity difference between the liquid and the crystal varies in $1/T$ or remains constant, two other closely related equations can be derived from the Adam-Gibbs theory [81] of cooperative relaxation [78] [74]:

$$\langle \tau \rangle = A_{AGF} \exp \left(\frac{Q_{AGF}}{RT (1 - T_{AGF}/T_f)} \right) \quad (47)$$

$$\langle \tau \rangle = A_{AGL} \exp \left(\frac{Q_{AGL}}{RT \ln(T_f/T_{AGL})} \right) \quad (48)$$

Equations (47) and (48) are respectively named the Adam-Gibbs-Fulcher (AGF) and Adam-Gibbs-Logarithmic (AGL) equations. It can be checked that, at equilibrium, by taking $T_f = T$ in equation (47), the VFT equation (44) is obtained. Hodge [74] (page 231) also mentions that the equilibrium version of the AGL equation:

$$\langle \tau \rangle = A_{AGL} \exp \left(\frac{Q_{AGL}}{RT \ln(T/T_{AGL})} \right) \quad (49)$$

is almost indistinguishable from a VFT equation. More details can be found in the review of Hodge and the works of Scherer [82] [83].

We will not go further in this very brief review of the relaxation theory as our modeling approach only relies on the above equations (41) to (48). The next subsection deals with the coupling of these equations with the thermodynamic ideal 2-state model presented in the 1.2 subsection.

2.2 Implementation of the coupled thermodynamic/kinetic modeling

The objective of this coupling is, starting from a temperature at which the liquid is in internal equilibrium, to simulate a cooling/reheating cycle under a prescribed $T(t)$ evolution. Here, constant heating and cooling rates, having possibly different values, were selected but modeling more complex temperature vs. time histories is not a problem in principle.

The main task consists in performing the time integration of the kinetic equation (41) describing the rate of change of the structural order parameter. This simple differential equation cannot be analytically integrated because of the complex dependence of the relaxation time on the thermodynamic variables. The integration is hence numerically performed using the following explicit forward finite difference scheme:

$$\frac{\xi_i - \xi_{i-1}}{\Delta t} = - \frac{\xi_i - \xi_{e,i}}{\tau_{i-1}} \quad (50)$$

Where Δt is the time step, i the current value of the time step index ($t = i \Delta t$) and τ_{i-1} the value of the relaxation time at the previous time step.

In the case of a constant rate γ of temperature change, the current temperature reads:

$$T_i = T_{ini} + i \Delta t \gamma \quad (51)$$

Using equation (50) and given the initial conditions, for each value of i , the value of ξ_i can be explicitly calculated from the knowledge of ξ_{i-1} and τ_{i-1} at the previous time step and the calculation of $\xi_{e,i}$ with the equilibrium condition (5).

It remains to evaluate the fictive temperature required to calculate the relaxation time τ_{i-1} if any of equations (45), (47) or (48) are used.

Coming back to the very definition of the fictive temperature, for a given internal state ξ of the glass at the temperature T , the corresponding fictive temperature T_f is the temperature at which the equilibrium liquid would have the same value of ξ . Hence, finding the fictive temperature $T_{f,i}$ associated to the current value of the internal variable ξ_i consists in solving the equation:

$$\xi_i = \xi_e(T_{f,i}) \quad (52)$$

This is numerically done in our Python program by using equation (5) and the *brentq* routine of the

scipy.optimize package. Let us emphasize that this numerical search raises no particular issue within the frame of the ideal 2-state model because ξ is a monotonous function of T . Hence, there is a complete bijection between the ξ and T_f values.

The assumption that the internal state of the glass could be represented by a single structural order parameter or fictive temperature value is an obvious simplification as discussed by Hodge [74] (page 219), different properties possibly having different fictive temperatures, but which has some merit in the present modeling focused on the enthalpic relaxation.

2.3 Review of experimental relaxation data of B_2O_3

Relaxation experiments were carried out over a wide temperature range from glass to equilibrium liquid, exploring 15 orders of magnitude of relaxation time.

Tauke et al. [84] made Ultra-Sonic (US) shear and longitudinal measurements in the liquid state from 823 to 1273 K. Bucaro et al. [85] measured the relaxation time in the glass state between 523 and 556 K using Pressure Jump Volume Relaxation (PJVR) and through the glass transition range between 583 and 746 K using Light Scattering Correlation Spectroscopy (LSCS). Sidebottom et al. [86] also used LSCS in the range 512-773 K. Fourteen years later, Sidebottom associated to other researchers [87] published a new dataset obtained by the same technique in the range 565-775 K. Dallari et al. [88] used a multi-speckle light scattering technique allowing to decrease the lower bound of the measuring range down to 493 K and covering the interval 493-563 K.

The average relaxation times from all studies are compared in Figure 9 using an Arrhenius representation. As the data are only presented as figures in references [86] [87] [88], it was necessary to digitize the graphs from the original articles. The data from [85] are relaxation times as they appear in the stretched exponential response function (equation (42)). They were converted to average relaxation times using equation (43).

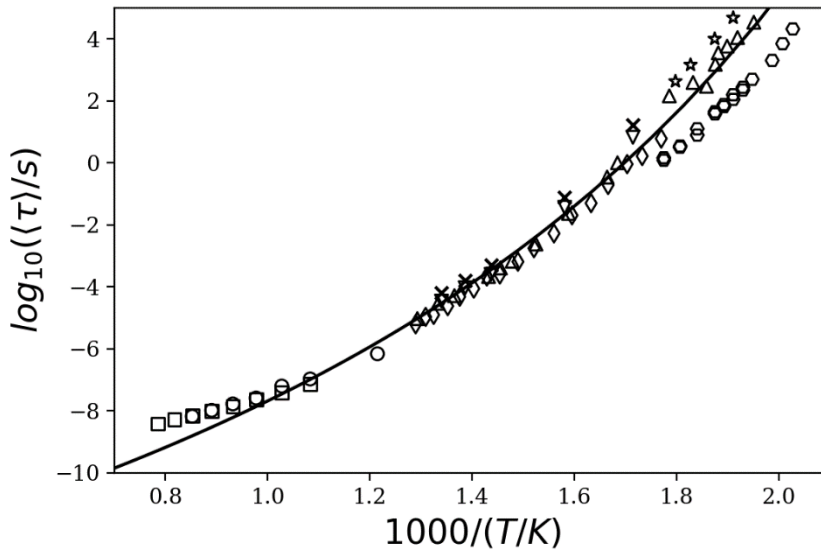


Figure 9. Arrhenius plot of the average relaxation time in B_2O_3 . Experiments: Tauke et al. [84] US shear mode (\square) US longitudinal mode (\circ), Bucaro et al. [85] LSCS mountain line (\times) LSCS anisotropic light (∇) PJVR (\star), Sidebottom et al. [86] LSCS (\triangle), Sidebottom et al. [87] LSCS (\diamond), Dallari et al. [88] LSCS (\circ). VFT equation with parameters from Hassan et al. [89] as listed in Table 5 (solid line).

The temperature dependence of the relaxation time has been analyzed by different authors [80] [78] [89] who have selected one or the other of the relaxation laws presented in subsection 2.1. These laws and the associated sets of parameters are compared in Table 5. Complete experimental data sets used to optimize the values of the parameters listed in Table 5 are not included in the original papers. It was

hence not possible to try to refit the data and, in the present work, we have used the relaxation laws and corresponding parameter sets as given in the original articles and listed in Table 5.

Table 5. Dependence of the relaxation time on temperature according to literature data.

Reference	Debolt et al. [80]	Moynihan et al. [78]	Hassan et al. [89]
Law	TNM	AGL	VFT
Parameters	$A_{TNM} = 1.51 \cdot 10^{-33} s$ $\chi = 0.4$ $\Delta h^* = 90 \times 4.184 kJ mol^{-1}$	$A_{AGL} = 7 \cdot 10^{-12} s$ $Q_{AGL} = 11.6 \times R kJ mol^{-1}$ $T_{AGL} = 286 K$	$A_{VFT} = 10^{-13.5} s$ $B_{VFT} = 35$ $T_{VFT} = 277 K$

2.4 Results and discussion of the coupled thermodynamic/kinetic modeling

The first step in tuning the combined thermodynamic/kinetic model consists in choosing an appropriate relaxation law.

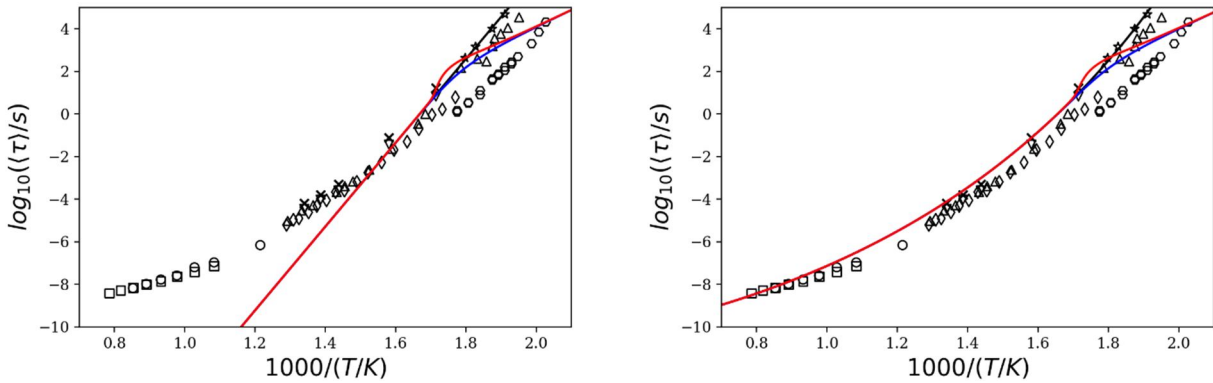
The TNM law adopted by Debolt et al. [80] suffers from several drawbacks.

From a practical point of view, as already pointed out by Hodge (see page 229 of [74]), the main drawback of this law lies in the fact that it reduces to an Arrhenius behavior (Figure 10a) above the glass transition temperature when the liquid is in internal equilibrium, i.e. for $T = T_f$, and strongly deviates from the VFT-like (Figure 9) temperature dependency shown by the experiments. By the way, it can be noticed that the relaxation time calculated with the TNM law during a cooling/heating cycle follows a hysteresis loop in the glass transition range due to the corresponding hysteresis loop followed by the fictive temperature itself (Figure 12b). This type of hysteresis, equally obtained using the AGL law (Figure 10b), has been already shown by Bisquert et al. [20] employing the same relaxation laws to simulate the glass transition in polymers.

In the glass transition range and at low temperatures, the AGL (Figure 10b) and TNM (Figure 10a) laws are very close. However, at high temperatures, the AGL law, which compares well with the experimental points, is far superior to the TNM law which fails completely in this temperature range.

From a more theoretical point of view, it can also be pointed out that the TNM law is purely phenomenological while the AGL law derives from the Adam-Gibbs theory of cooperative relaxation and hence has a more solid basis. Moreover, following Sales [90], it can be noticed that the order of magnitude of the prefactor $A_{AGL} = 7 \cdot 10^{-12} s$ in the AGL law is comparable to a phonon or atomic vibration time and hence has a sounder physical interpretation than the extremely small prefactor $A_{TNM} = 1.51 \cdot 10^{-33} s$ that seems hard to justify by any explanation apart from its ability to fit the data.

For all the above reasons the TNM law was hence not selected in the present work.



a) TNM Law with parameters from Debolt et al. [80] as listed in Table 5 b) AGL Law with parameters from Moynihan et al. [78] as listed in Table 5

Figure 10. Arrhenius plot of the average relaxation time in B_2O_3 . Experiments: Tauke et al. [84] US shear mode (\square)

US longitudinal mode (○), Bucaro et al. [85] LSCS mountain line (×) LSCS anisotropic light (▽) PJVR (★), Sidebottom et al. [86] LSCS (Δ), Sidebottom et al. [87] LSCS (◇), Dallari et al. [88] LSCS (◻). Relaxation laws, internal equilibrium (black curves), cooling at 10 K/min (blue curves), heating at 10 K/min after prior cooling at 10 K/min (red curves). Calculations performed with the recommended values of the liquid two-state model A, B parameters given in Table 6.

So, we are left with the choice between the AGL and VFT equations, both providing reasonable fits to the experimental data as can be seen from the comparison of Figure 9 with Figure 10b. At this stage, a deeper insight can be gained from the comparison of the evolutions of the liquid configurational heat capacity vs. temperature using these two laws. Such a comparison is presented for data measured on heating at 10 K/min after prior cooling at 10 (Figure 11a and b) or 80 (Figure 11c and d) K/min and shows that the AGL law gives the best fit of the heat capacity rise at the glass transition and in particular of the sub- T_g endotherm seen in Figure 11d. This is not surprising considering, as already mentioned in subsection 2.1 that the VFT law, which does not depend on the state of the glass, is hence unable to account from subtle non-linear relaxation effect.

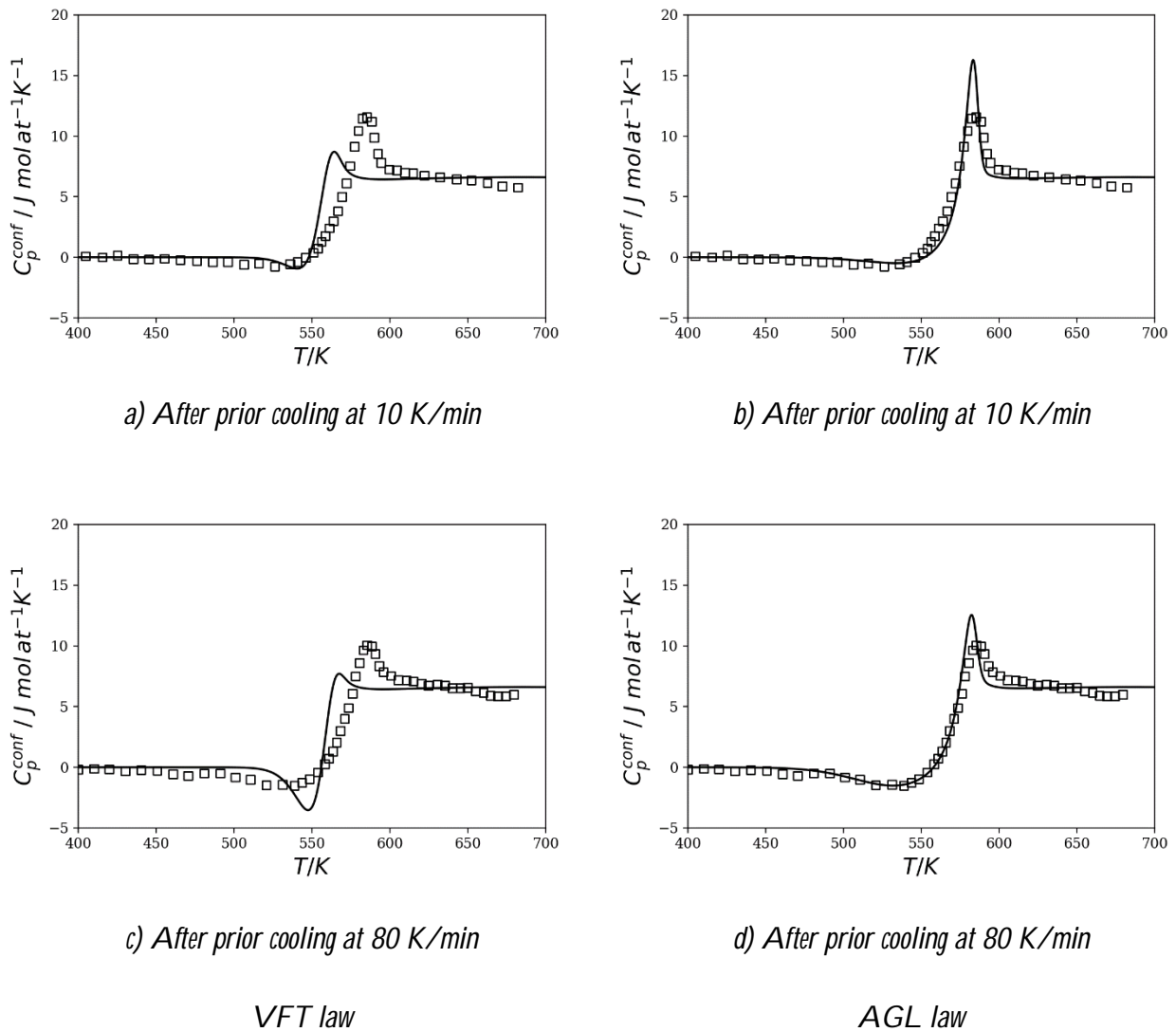


Figure 11. Liquid configurational heat capacity vs. temperature in the glass transition range on heating at 10 K/min. (□) Experimental points from Moynihan et al. [65]. Black curve = modeling from this work with the recommended values of the liquid two-state model A, B parameters given in Table 6.

In conclusion, the AGL law, which has a firm theoretical basis, for which the order of magnitude of the parameters remains “physical”, which is able to faithfully simulate relaxation in the glass transition range

and tends towards the VFT law at equilibrium, was adopted in the present work.

Having chosen the relaxation law, the variation of the fictive temperature could be calculated as a function of the cooling rate. Fictive temperatures of 540 and 520 K (Table 2) were found to approximately correspond to cooling rates of respectively 1 and 0.025 K/min. This information was used for the optimization of the A and B coefficient of the two-state model.

However, the problem is strongly over constrained considering, on one side, the large number of experimental data available over a large temperature range and on the other side that, because of equations (36) and (40), there is only one degree of freedom left for adjusting the Gibbs energy difference between the solid- and liquid-like states. Hence, it was not possible to achieve a good fit of all data.

As already mentioned in subsection 1.5, the value of B was set manually. The initial value of B was chosen to be equal to the communal entropy $B = -R$ and the corresponding initial value of A was computed by numerical solution of equation (40). Then the kinetic simulation was run. We prioritized two criteria in assessing the quality of the calculated results: i) a realistic calculated value of the frozen-in entropy and (ii) a good fit of the heat capacity measurements in the glass transition range. The process was repeated by trial and error, changing the B value until the two above criteria were approximately fulfilled.

The finally selected values of the A and B coefficients are presented in Table 6. These values provide a prediction of the residual entropy with a relative uncertainty around 10% (Table 2) and a reasonable fit of the heat capacity data in the glass transition range (Figure 11b and d).

Table 6. Values of the parameters of the two-state model of the liquid selected in this work.

$A / J \text{ mol at}^{-1}$	15248.47522169
$B / J \text{ mol at}^{-1} K^{-1}$	$-\frac{3}{4}R$
$A' / J \text{ mol at}^{-1}$	2520

The A' parameter can now be estimated. The enthalpy of the vitrification reaction (equation 32) is first calculated at 0 K (last line of Table 1) from its value at 298 K measured by Johnson and Hubbard [72] and the enthalpy increments of the crystal and the glass between 0 and 298 K from the present modeling. The calculated value is: $\Delta_{vitr} H_0^\circ = 17.7 \text{ kJ mol}^{-1} \approx 72\% \Delta_m H_{723}$. Rigorously, the estimation of A' requires to know the experimental condition of elaboration of the glass used by Johnson and Hubbard. In their article, it is only specified that it was obtained by slowly lowering the temperature of a “clear viscous melt” down to room temperature. We have assumed that such cooling corresponded to a rate of 1 K/min. A frozen-in configurational enthalpy of 5.1 kJ mol^{-1} is calculated with the model for this cooling rate leading to the estimate given in Table 6, $A' = 12.6 \text{ kJ mol}^{-1} = 2520 \text{ J mol at}^{-1}$.

The very similar evolutions of the structural order parameter ξ and the fictive temperature during a cooling/heating cycle at 10 K/min are plotted through the glass transition range in Figure 12a and b showing the characteristic hysteresis loops of both quantities. The corresponding evolution of the configurational heat capacity is plotted over a larger temperature interval in Figure 12c. Under internal equilibrium conditions, the configurational heat capacity vanishes below approximately 200 K due to the purely thermodynamic 2-state description, whereas on cooling at 10 K/min, it cancels out below 450 K due to the “real glass transition” of kinetic origin. The kinetic calculation was stopped at 310 K to avoid the numerical divergence of the relaxation law (equation 48) below this bound.

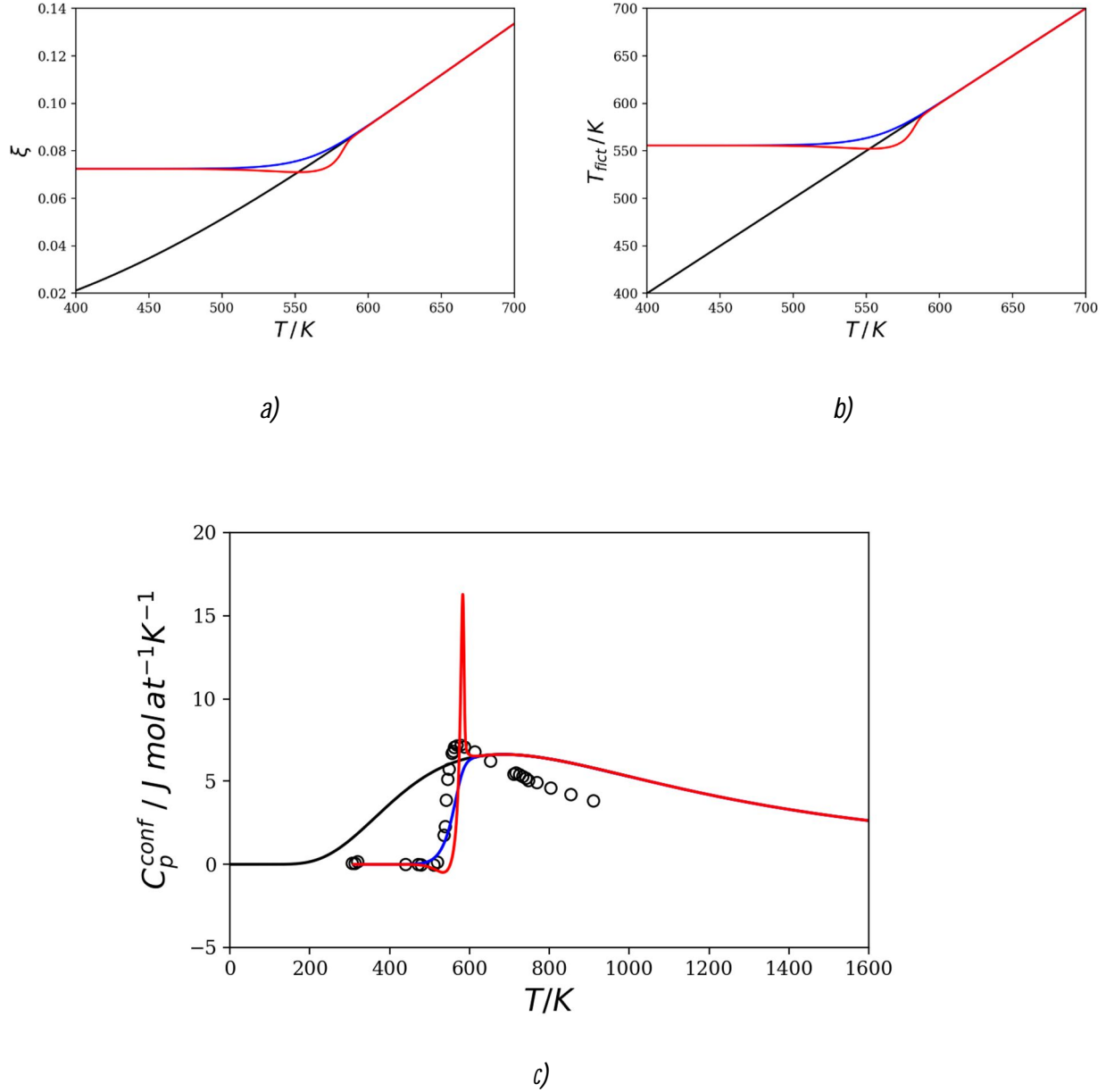


Figure 12. Evolutions of a) the structural order parameter ξ (= fraction of liquid-like entities) b) the fictive temperature and c) the configurational heat capacity through the glass transition range under internal equilibrium conditions (black curve), on cooling from the liquid at 10 K/min (blue curve) and on reheating the glass at the same rate (red curve). The fictive temperature of the glass obtained on cooling is $T^* = 555.6$ K. (\circ) adiabatic calorimetry measurements by Shmidt [60] after subtraction of the vibrational contribution calculated with our modeling.

To give a fair overview of the model performance, it is necessary to add that the good fit of the heat capacity evolutions measured by DSC at constant rate in the glass temperature range, and the reasonable calculation of the residual zero-point entropy, is obtained at the expense of an overestimation of the configurational heat capacity of the equilibrium liquid between 700 and 910 K (Figure 12c) compared to the adiabatic calorimetry measurements of Shmidt [60]. The liquid enthalpy increments, which are not consistent with the DSC and adiabatic heat capacity data are also overestimated by our modeling (solid line Figure 4). As a final test of the present modeling, the calculated entropy curves for the various phases are plotted and compared to the entropy tabulated values from the JANAF tables in Figure 13.

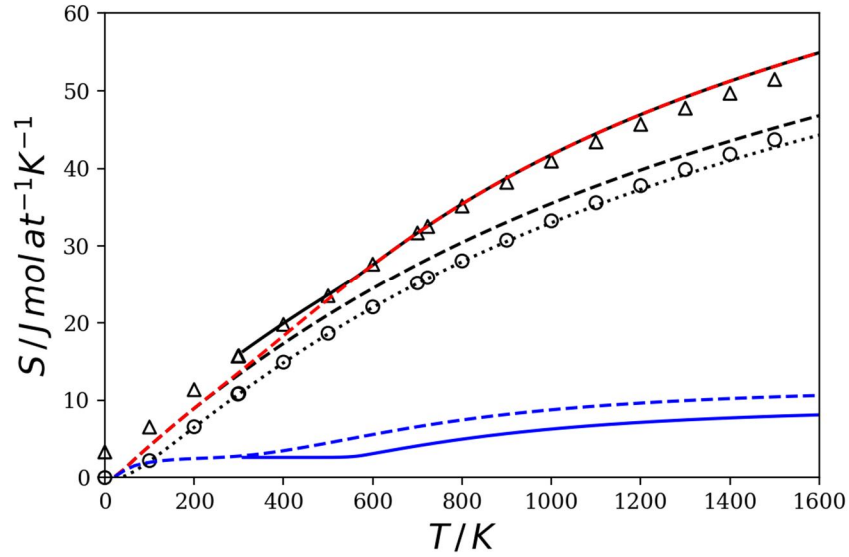


Figure 13. Entropy vs. temperature, symbols are numerical values from JANAF tables [69] and lines are calculated with the present modeling; crystal phase (\circ and black dotted line), "sol" phase (black dashed line), liquid/glass phase on cooling at 10 K/min (Δ and solid black line) and at equilibrium (red dashed line). Configurational entropy of the liquid/glass phase on cooling at 10 K/min (solid blue line). Entropy difference between the liquid at equilibrium and the crystal (blue dashed line). Note that the "sol" phase obeys the 3^d law while the liquid/glass" phase cooled at 10 K/min has a non-zero residual entropy as shown by the constant value of the solid blue line below 550 K. Additionally, it is seen that the excess entropy of the liquid/glass, namely the calculated entropy difference (blue dashed line) between the liquid/glass at equilibrium and the crystal, only vanishes at 0 K.

Conclusions and outlook

To our knowledge, this is the first time that a coupled thermodynamic/kinetic CALPHAD type modeling of the glass transition for a glass forming unary substance is proposed. In this modeling, the vibrational contributions to the thermodynamic functions of the crystal and the liquid/glass phases are classically modeled using weighed sums of Einstein functions while the configurational contributions to the liquid/glass phase functions are described using a single internal variable within the frame of the ideal two-state model. The kinetic freezing of this internal variable on cooling is calculated with an Adam-Gibbs logarithmic relaxation law.

With the selected set of parameter values, the model is able to simulate the evolution of the thermodynamic functions with temperature in the glass transition range where they depart from their equilibrium values. However, complete agreement with all available experimental data was not achieved due to i) some conflicting data and ii) the existence of several constraints which drastically limits the number of degrees of freedom during the optimization of the parameter values.

It is our belief that this first modeling can be greatly improved. Let us mention few possible improvements and extensions.

First, at the present state of the modeling, the description of the liquid/glass as a mixture of solid- and liquid-like entities is purely formal and nothing is implied on the real physical nature of these entities. However, it is known from Raman scattering studies [89] that the liquid is made of threefold six-member planar B_3O_6 boroxol rings and chains of BO_3 triangles. The fraction of boroxol rings remains constant around 60% at the glass state below the glass transition temperature T_g . As the temperature is increased above T_g , an increasing number of rings are opening up and the boroxol fraction decreases reaching around 45% at the melting point. It might therefore be interesting to adopt the fraction of one (or the other) of the organizational units as a potential structural order parameter of the liquid. This idea is obviously not new and a microscopic model [91] describing the liquid as a mixture of boroxol rings and planar triangles has already been used to interpret Raman scattering [92] and relaxation [93] experiments.

More generally, thermodynamic descriptions relying on the structural units defining the short and medium range orders in glass forming liquids are the basis of the “constitutional model” of Conradt [94] [95] [96], the “Associate Solution Model” of Vedischeva et al. [97] [98] [99] [100]. The concept of “associate-solution model” is also widely used for modeling liquid solutions in the CALPHAD approach [101]. However, it is worth emphasizing that the use of structural information will put additional constraints in the already over constrained optimization process as, for example, the evolution of the order parameter such as the one presented in Figure 12a could then be compared to available structural data.

Second, another interesting development would be to introduce the $(-p, V)$ couple of conjugate variables in the present model considering that pressure should affect both the thermodynamic and kinetic descriptions. On the thermodynamic side, at ambient pressure, the evolution of the specific volume [15], the shear and longitudinal moduli [102], the thermal expansion and isothermal compressibility [103] have been measured through the glass transition range. A complete thermodynamic modeling of the $p - T$ unary phase diagram up to 8 GPa and 1900 K has been published by Solozhenko et al. [104] including a list of *in situ* studies of B_2O_3 liquid/glass under high pressure. It is known that on increasing pressure, the boron short range order changes in a similar way for both the crystalline and the liquid/glass phases with the coordination number of boron atoms increasing from three to four [105]. The thermodynamic pressure modeling will necessarily require to use a more sophisticated model for the liquid possibly having more than one internal variable considering that the Defay-Prigogine ratio is equal to 4.7 [106] for B_2O_3 and hence larger than one. In this respect, a liquid model with two internal variables was suggested by Agren for glycerol in his pioneering article [11] and more interesting, Leidecker et al. [107] have long ago proposed an analysis of structural rearrangements in vitreous B_2O_3 using a three-state model, or more precisely a degenerate two-state model with a single ground state and a twofold degenerate excited state which is characterized by different volumes. On the kinetic side, Rault [108] has recently proposed a modified VFT law to take into account the effect of pressure on the relaxation times in glass formers and Masiewicz et al. [109] have formulated a temperature-volume representation of the Adam-Gibbs model.

The third perspective is the multicomponent extension of such a coupled thermodynamic/kinetic modeling. One of the difficulty will be to assess the effect of the compositional change on the relaxation kinetics because it is known, for example, that increasing the alkali content in Na_2O-SiO_2 and K_2O-SiO_2 binary systems narrows the spectrum of relaxation times. (see figure 5 of [5]).

Acknowledgments

A. L. Voskov, I. B. Kutsenok, G. F. Voronin (Lomonosov University Moscow) for making their CpFit program freely available. Jean-Luc Garden (Institut Néel Grenoble) for inspiring discussions on thermodynamics and the glass transition and for drawing my attention on Bisquert's articles. Marc Gailhanou (IM2NP Marseille) for invaluable help in numerical computing and Python programming. Jacques Rogez (IM2NP Marseille) for help in some calculations and useful comments on the manuscript. This work started from discussions with Jacques Rogez and Sophie Schuller (CEA Marcoule) in the subgroup “Thermodynamics of Glasses” of the French thematic network “Thermodynamique des Matériaux Hautes Températures” (ThermatHT) – GDR CNRS n°3584. This article was written during the COVID-19 crisis and Marc Barrachin (IRSN Cadarache) and Dominique de Ligny (IGC Erlangen) are gratefully acknowledged for sending me key-articles when French university libraries were closed.

Abbreviations

AGF: Adam-Gibbs Fulcher relaxation law.

AGL: Adam-Gibbs Logarithmic relaxation law.

KWW: Kohlrausch-William-Watts decay function.

LSCS: Light Scattering Correlation Spectroscopy.

PJVR: Pressure Jump Volume Relaxation.

TLS: Two-Level System.

TNM: Tool-Narayanaswamy-Moynihan relaxation law.

TIP: Thermodynamics of Irreversible Processes.

VFT: Vogel-Fulcher-Tammann relaxation law.

Data availability

The raw data required to reproduce these findings are available to download from:

<https://data.mendeley.com/datasets/xvzmjp2x7d/draft?a=ca7c4d31-2dca-40af-aeae-013a86852db2>

<https://data.mendeley.com/datasets/mpygv2xdpc/draft?a=5b3de133-1021-409d-9201-d0d8ea2a1f2b>

References

- [1] W. Kauzmann, The Nature of the Glassy State and the Behavior of Liquids at Low Temperatures., *Chem. Rev.* 43 (1948) 219–256. <https://doi.org/10.1021/cr60135a002>.
- [2] R.O. Davies, G.O. Jones, The Irreversible Approach to Equilibrium in Glasses, *Proc. R. Soc. A Math. Phys. Eng. Sci.* 217 (1953) 26–42. <https://doi.org/10.1098/rspa.1953.0044>.
- [3] R.O. Davies, G.O. Jones, Thermodynamic and kinetic properties of glasses, *Adv. Phys.* 2 (1953) 370–410. <https://doi.org/10.1080/00018735300101252>.
- [4] I. Prigogine, R. Defay, *Chemical Thermodynamics*, Longmans, Greens and Co., 1954.
- [5] S. V. Nemilov, *Thermodynamic and Kinetic Aspects of the Vitreous State*, CRC Press, 1995.
- [6] M. Palumbo, L. Battezzati, Thermodynamics and kinetics of metallic amorphous phases in the framework of the CALPHAD approach, *Calphad Comput. Coupling Phase Diagrams Thermochem.* 32 (2008) 295–314. <https://doi.org/10.1016/j.calphad.2007.12.002>.
- [7] C.A. Angell, K.J. Rao, Configurational excitations in condensed matter, and the “Bond Lattice” model for the liquid-glass transition, *J. Chem. Phys.* 57 (1972) 470–481. <https://doi.org/10.1063/1.1677987>.
- [8] I.S. Gutzow, J.W.P. Schmelzer, *The Vitreous State: Thermodynamics, Structure, Rheology, and Crystallization*, 2nd ed., Springer Verlag Berlin Heidelberg, 2013.
- [9] P. Benigni, Thermodynamic analysis of the classical lattice-hole model of liquids, *J. Non. Cryst. Solids.* 534 (2020) 119942. <https://doi.org/10.1016/j.jnoncrysol.2020.119942>.
- [10] P.W. Guan, Z.K. Liu, A physical model of thermal vacancies within the CALPHAD approach, *Scr. Mater.* 133 (2017) 5–8. <https://doi.org/10.1016/j.scriptamat.2017.02.002>.
- [11] J. Ågren, Thermodynamics of Supercooled Liquids and their Glass Transition, *Phys. Chem. Liq.* 18 (1988) 123–139. <https://doi.org/10.1080/00319100701344644>.
- [12] J. Agren, B. Cheynet, M.T. Clavaguera-mora, K. Hack, J. Hertz, F. Sommer, U. Kattner, Workshop on thermodynamic models and data for pure elements and other endmembers of solutions, *Calphad.* 19 (1995) 449–480. [https://doi.org/10.1016/0364-5916\(96\)00003-X](https://doi.org/10.1016/0364-5916(96)00003-X).
- [13] C. a. Becker, J. Ågren, M. Baricco, Q. Chen, S. a. Decterov, U.R. Kattner, J.H. Perepezko, G.R. Pottlacher, M. Selleby, Thermodynamic modelling of liquids: CALPHAD approaches and contributions from statistical physics, *Phys. Status Solidi.* 52 (2014) 33–52. <https://doi.org/10.1002/pssb.201350149>.
- [14] Z. Li, S. Bigdeli, H. Mao, Q. Chen, M. Selleby, Thermodynamic evaluation of pure Co for the third generation of thermodynamic databases, *Phys. Status Solidi Basic Res.* 254 (2017). <https://doi.org/10.1002/pssb.201600231>.
- [15] P.B. Macedo, W. Capps, T.A. Litovitz, Two-□ State Model for the Free Volume of Vitreous B₂O₃, *J. Chem. Phys.* 44 (1966) 3357–3364. <https://doi.org/10.1063/1.1727238>.
- [16] S.A. Langer, A.T. Dorsey, J.P. Sethna, Entropy distribution of a two-level system: An asymptotic analysis, *Phys. Rev. B.* 40 (1989) 345–352. <https://doi.org/10.1103/PhysRevB.40.345>.
- [17] S.A. Langer, J.P. Sethna, E.R. Grannan, Nonequilibrium entropy and entropy distributions, *Phys. Rev. B.* 41 (1990) 2261–2278. <https://doi.org/10.1103/PhysRevB.41.2261>.
- [18] V. Halpern, J. Bisquert, The effect of the cooling rate on the fictive temperature in some model glassy systems, *J. Chem. Phys.* 114 (2001) 9512–9517. <https://doi.org/10.1063/1.1370961>.
- [19] J. Bisquert, Master equation approach to the non-equilibrium negative specific heat at the glass transition, *Am. J. Phys.* 73 (2005) 735–741. <https://doi.org/10.1119/1.1891173>.
- [20] J. Bisquert, F. Henn, J.C. Giuntini, A simple model of entropy relaxation for explaining effective activation energy behavior below the glass transition temperature, *J. Chem. Phys.* 122 (2005) 1–9. <https://doi.org/10.1063/1.1858862>.
- [21] A. Takada, R. Conradt, P. Richet, Residual entropy and structural disorder in glass: A two-level model and a review of spatial and ensemble vs. temporal sampling, *J. Non. Cryst. Solids.* 360 (2013) 13–20. <https://doi.org/10.1016/j.jnoncrysol.2012.10.002>.
- [22] H. Jabraoui, S. Ouaskit, J. Richard, J.-L. Garden, Determination of the entropy production during glass transition: Theory and experiment, *J. Non. Cryst. Solids.* 533 (2020) 119907. <https://doi.org/10.1016/j.jnoncrysol.2020.119907>.
- [23] M.I. Ojovan, W. (Bill) E. Lee, Connectivity and glass transition in disordered oxide systems, *J. Non.*

- Cryst. Solids. 356 (2010) 2534–2540. <https://doi.org/10.1016/j.jnoncrsol.2010.05.012>.
- [24] D.S. Sanditov, M.I. Ojovan, On relaxation nature of glass transition in amorphous materials, *Phys. B Condens. Matter.* 523 (2017) 96–113. <https://doi.org/10.1016/j.physb.2017.08.025>.
- [25] Q. Chen, B. Sundman, Modeling of Thermodynamic Properties for Bcc, Fcc, Liquid, and Amorphous Iron, *J. Phase Equilibria.* 22 (2001) 631–644. <https://doi.org/10.1361/105497101770332442>.
- [26] S. Bigdeli, H. Mao, M. Selleby, On the third-generation Calphad databases: An updated description of Mn, *Phys. Status Solidi Basic Res.* 252 (2015) 2199–2208. <https://doi.org/10.1002/pssb.201552203>.
- [27] A.V. Khvan, A.T. Dinsdale, I.A. Uspenskaya, M. Zhilin, T. Babkina, A.M. Phiri, A thermodynamic description of data for pure Pb from 0 K using the expanded Einstein model for the solid and the two state model for the liquid phase, *Calphad.* 60 (2018) 144–155. <https://doi.org/10.1016/j.calphad.2017.12.008>.
- [28] S. Bigdeli, Q. Chen, M. Selleby, A New Description of Pure C in Developing the Third Generation of Calphad Databases, *J. Phase Equilibria Diffus.* 39 (2018) 832–840. <https://doi.org/10.1007/s11669-018-0679-3>.
- [29] A. V. Khvan, T. Babkina, A.T. Dinsdale, I.A. Uspenskaya, I. V. Fartushna, A.I. Druzhinina, A.B. Syzdykova, M.P. Belov, I.A. Abrikosov, Thermodynamic properties of tin: Part I Experimental investigation, ab-initio modelling of α -, β -phase and a thermodynamic description for pure metal in solid and liquid state from 0 K, *Calphad Comput. Coupling Phase Diagrams Thermochem.* 65 (2019) 50–72. <https://doi.org/10.1016/j.calphad.2019.02.003>.
- [30] O. Tolochko, J. Ågren, Thermodynamic properties of supercooled Fe-B liquids—A theoretical and experimental study, *J. Phase Equilibria.* 21 (2000) 19–24. <https://doi.org/10.1361/105497100770340372>.
- [31] S. Bigdeli, M. Selleby, A thermodynamic assessment of the binary Fe-Mn system for the third generation of Calphad databases, *Calphad Comput. Coupling Phase Diagrams Thermochem.* 64 (2019) 185–195. <https://doi.org/10.1016/j.calphad.2018.11.011>.
- [32] M.H. Cohen, G.S. Grest, A New Free-Volume Theory Of The Glass Transition, *Ann. N. Y. Acad. Sci.* 371 (1981) 199–209. <https://doi.org/10.1111/j.1749-6632.1981.tb55661.x>.
- [33] M.H. Cohen, G.S. Grest, The nature of the glass transition, *J. Non. Cryst. Solids.* 61–62 (1984) 749–759. [https://doi.org/10.1016/0022-3093\(84\)90634-3](https://doi.org/10.1016/0022-3093(84)90634-3).
- [34] J. Frenkel, *Kinetic Theory of Liquids*, Oxford University Press, Oxford, 1946.
- [35] K. Trachenko, V. V. Brazhkin, Collective modes and thermodynamics of the liquid state, *Reports Prog. Phys.* 79 (2016) 016502. <https://doi.org/10.1088/0034-4885/79/1/016502>.
- [36] G. Deffrennes, N. Jakse, C.M.S. Alvares, I. Nuta, A. Pasturel, A. Khvan, A. Pisch, Thermodynamic modelling of the Ca–O system including 3rd generation description of CaO and CaO₂, *Calphad Comput. Coupling Phase Diagrams Thermochem.* 69 (2020). <https://doi.org/10.1016/j.calphad.2020.101764>.
- [37] J.A. Golczewski, H.J. Seifert, F. Aldinger, A Thermodynamic Model of Amorphous Silicates, *Calphad.* 22 (1998) 381–396.
- [38] N. Stolen, Svein, Grande, Tor, Allan, *Chemical Thermodynamics of Materials*, Wiley, 2004. <https://doi.org/10.1002/0470092688>.
- [39] V. Holten, M.A. Anisimov, Entropy-driven liquid-liquid separation in supercooled water, (2012). <https://doi.org/10.1038/srep00713>.
- [40] E.G. Ponyatovsky, O.I. Barkalov, Pressure—induced amorphous phases, *Mater. Sci. Reports.* 8 (1992) 147–191. [https://doi.org/10.1016/0920-2307\(92\)90007-N](https://doi.org/10.1016/0920-2307(92)90007-N).
- [41] H. Tanaka, General view of a liquid-liquid phase transition, *Phys. Rev. E.* 62 (2000) 6968–6976. <https://doi.org/10.1103/PhysRevE.62.6968>.
- [42] M.H. Cohen, D. Turnbull, Molecular Transport in Liquids and Glasses, *J. Chem. Phys.* 31 (1959) 1164–1169. <https://doi.org/10.1063/1.1730566>.
- [43] C.A. Angell, Formation of Glasses from Liquids and Biopolymers, *Science* (80-.). 267 (1995) 1924–1935. <https://doi.org/10.1126/science.267.5206.1924>.
- [44] P. Debenedetti, F. Stillinger, Supercooled liquids and the glass transition, *Nature.* 410 (2001) 259–

267. <https://doi.org/10.1038/35065704>.
- [45] F. Semerianov, P.D. Gujrati, Configurational entropy and its crisis in metastable states: Ideal glass transition in a dimer model as a paradigm of a molecular glass, *Phys. Rev. E - Stat. Nonlinear, Soft Matter Phys.* 72 (2005) 1–23. <https://doi.org/10.1103/PhysRevE.72.011102>.
- [46] P.D. Gujrati, Energy Gap Model of Glass Formers: Lessons Learned from Polymers, in: *Model. Simul. Polym.*, Wiley-VCH Verlag GmbH & Co. KGaA, Weinheim, Germany, 2010: pp. 433–495. <https://doi.org/10.1002/9783527630257.ch10>.
- [47] T.L. Hill, *An Introduction To Statistical Thermodynamics*, Dover Publications, Inc., New York, 1986. <https://doi.org/10.1142/9789812385147>.
- [48] G.F. Voronin, I.B. Kutsenok, Universal method for approximating the standard thermodynamic functions of solids, *J. Chem. Eng. Data.* 58 (2013) 2083–2094. <https://doi.org/10.1021/jc400316m>.
- [49] A.L. Voskov, I.B. Kutsenok, G.F. Voronin, CpFit program for approximation of heat capacities and enthalpies by Einstein-Planck functions sum, *Calphad Comput. Coupling Phase Diagrams Thermochem.* 61 (2018) 50–61. <https://doi.org/10.1016/j.calphad.2018.02.001>.
- [50] A.L. Voskov, G.F. Voronin, I.B. Kutsenok, N.Y. Kozin, Thermodynamic database of zeolites and new method of their thermodynamic properties evaluation for a wide temperature range, *Calphad Comput. Coupling Phase Diagrams Thermochem.* 66 (2019) 101623. <https://doi.org/10.1016/j.calphad.2019.04.008>.
- [51] A.Q. Tool, Relaxation of stresses in annealing glass, *J. Res. Natl. Bur. Stand.* (1934). 34 (1945) 199. <https://doi.org/10.6028/jres.034.007>.
- [52] A.Q. Tool, Relation Between Inelastic Deformability and Thermal Expansion of Glass in Its Annealing Range, *J. Am. Ceram. Soc.* 29 (1946) 240–253. <https://doi.org/10.1111/j.1151-2916.1946.tb11592.x>.
- [53] M. Goldstein, Statistical Thermodynamics Of Configurational Properties, *Ann. N. Y. Acad. Sci.* 279 (1976) 68–77. <https://doi.org/10.1111/j.1749-6632.1976.tb39694.x>.
- [54] S.A. Decterov, V. Swamy, I.-H. Jung, Thermodynamic modeling of the B₂O₃ – SiO₂ and B₂O₃ – Al₂O₃ systems, *Int. J. Mater. Res.* 98 (2007) 987–994. <https://doi.org/10.3139/146.101555>.
- [55] S. Chen, J. Su, Y. Wang, Y. Tang, X. He, Thermodynamic assessment of B₂O₃–MgO binary system, *Calphad.* 51 (2015) 67–74. <https://doi.org/10.1016/j.calphad.2015.07.004>.
- [56] X. Fan, L.M. Su, G.M. Cai, H.S. Liu, Z.P. Jin, Experimental determination and thermodynamic calculation of BaO–In₂O₃–B₂O₃ system, *Calphad.* 55 (2016) 281–293. <https://doi.org/10.1016/j.calphad.2016.11.001>.
- [57] S.A. Utlak, T.M. Besmann, Thermodynamic assessment of the Na₂O–Al₂O₃–SiO₂–B₂O₃ pseudo-binary and -ternary systems, *J. Chem. Thermodyn.* 130 (2019) 251–268. <https://doi.org/10.1016/j.jct.2018.09.001>.
- [58] K.K. Kelley, The Specific Heats at Low Temperatures of Crystalline Boric Oxide, Boron Carbide and Silicon Carbide 1, *J. Am. Chem. Soc.* 63 (1941) 1137–1139. <https://doi.org/10.1021/ja01849a072>.
- [59] E.C. Kerr, H.N. Hersh, H.L. Johnston, Low Temperature Heat Capacities of Inorganic Solids. 1 II. The Heat Capacity of Crystalline Boric Oxide from 17 to 300°K., *J. Am. Chem. Soc.* 72 (1950) 4738–4740. <https://doi.org/10.1021/ja01166a108>.
- [60] N.E. Shmidt, Heat capacity and heat of fusion of crystalline boron oxide, *Russ. J. Inorg. Chem.* 11 (1966) 241–247.
- [61] J.C. Southard, The Thermal Properties of Crystalline and Glassy Boron Trioxide, *J. Am. Chem. Soc.* 63 (1941) 3147–3150. <https://doi.org/10.1021/ja01856a073>.
- [62] V.A. Turdakin, V. V. Tarasov, Heat capacity of boric oxide and sodium borate glasses at low temperatures, *Russ. J. Coord. Chem.* 11 (1966) 501–502.
- [63] P. Richet, D. de Ligny, E.F. Westrum, Low-temperature heat capacity of GeO₂ and B₂O₃ glasses: thermophysical and structural implications, *J. Non. Cryst. Solids.* 315 (2003) 20–30. [https://doi.org/10.1016/S0022-3093\(02\)01581-8](https://doi.org/10.1016/S0022-3093(02)01581-8).
- [64] S.B. Thomas, G.S. Parks, Studies on Glass. VI. Some Specific Heat Data on Boron Trioxide, *J. Phys. Chem.* 35 (1931) 2091–2102. <https://doi.org/10.1021/j150325a016>.

- [65] C.T. Moynihan, A.J. Easteal, M.A. Debolt, J. Tucker, Dependence of the Fictive Temperature of Glass on Cooling Rate, *J. Am. Ceram. Soc.* 8 (1976) 12–16. <https://doi.org/10.1111/j.1151-2916.1976.tb09376.x>.
- [66] R.M. Krasovitskaya, P.B. Kantor, L.S. Kan, V. V. Kandyba, L.M. Kutsyna, E.N. Fomichev, Th, The Enthalpy and Heat Capacity of Boron Oxide between 1000° and 2200°K, *Russ. J. Phys. Chem.* 35 (1961) 737–738.
- [67] E.E. Shpil'rain, K.A. Yakimovich, A.F. Tsitsarkin, D.N. Kagan, L.S. Barkhatov, V.A. Fomin, Y. Tsigenkhagen, Comprehensive Investigation of the Thermophysical Properties of Molten Boron Oxide, *Fluid Mech. – Sov. Res.* 3 (1974) 29–36.
- [68] J. Klein, F. Müller, Measurement of the enthalpy of mixing of the liquid system CaO-B₂O₃ by drop calorimetry, *High Temp. High Press.* 19 (1987) 201–209.
- [69] M. Chase Jr, NIST-JANAF Thermochemical Tables Fourth Edition, *J. Phys. Chem. Ref. Data, Monogr.* 9. (1998). <https://janaf.nist.gov/janaf4pdf.html>.
- [70] J.D. Cox, D.D. Wagman, V.A. Medvedev, CODATA - Key Values for Thermodynamics, Hemisphere Publishing Corporation, New York, Washington, Philadelphia, London 1989., 1989.
- [71] L.V. Gurvich, I.V. Veyts, V.S. Iorish, C.B. Alcock, Thermodynamic Properties of Individual Substances, Volume 3, Parts 1 and 2, 4th ed., CRC Press, 1994.
- [72] G.K. Johnson, W.N. Hubbard, The enthalpies of formation of crystalline and amorphous boric oxide and orthoboric acid, *J. Chem. Thermodyn.* 1 (1969) 459–468. [https://doi.org/10.1016/0021-9614\(69\)90004-4](https://doi.org/10.1016/0021-9614(69)90004-4).
- [73] G.P. Johari, Contributions to the entropy of a glass and liquid, and the dielectric relaxation time, *J. Chem. Phys.* 112 (2000) 7518–7523. <https://doi.org/10.1063/1.481349>.
- [74] I.M. Hodge, Enthalpy relaxation and recovery in amorphous materials, *J. Non. Cryst. Solids.* 169 (1994) 211–266. [https://doi.org/10.1016/0022-3093\(94\)90321-2](https://doi.org/10.1016/0022-3093(94)90321-2).
- [75] E.-J. Donth, The Glass Transition - Relaxation Dynamics in Liquids and Disordered Materials, Springer Berlin Heidelberg, Berlin, Heidelberg, 2001. <https://doi.org/10.1007/978-3-662-04365-3>.
- [76] J. Möller, I. Gutzow, J.W.P. Schmelzer, Freezing-in and production of entropy in vitrification, *J. Chem. Phys.* 125 (2006). <https://doi.org/10.1063/1.2346673>.
- [77] P.J. Carroll, G.D. Patterson, The distribution of relaxation frequencies from photon correlation spectroscopy near the glass transition, *J. Chem. Phys.* 82 (1985) 9–13. <https://doi.org/10.1063/1.448741>.
- [78] C.T. Moynihan, S.N. Crichton, S.M. Opalka, Linear and non-linear structural relaxation, *J. Non. Cryst. Solids.* 131–133 (1991) 420–434. [https://doi.org/10.1016/0022-3093\(91\)90335-4](https://doi.org/10.1016/0022-3093(91)90335-4).
- [79] I. Gutzow, J.W.P. Schmelzer, B. Petroff, Phenomenological theories of glass transition: Classical approaches, new solutions and perspectives, *J. Non. Cryst. Solids.* 354 (2008) 311–324. <https://doi.org/10.1016/j.jnoncrysol.2007.07.042>.
- [80] M.A. Debolt, A.J. Easteal, P.B. Macedo, C.T. Moynihan, Analysis of Structural Relaxation in Glass Using Rate Heating Data, *J. Am. Ceram. Soc.* 59 (1976) 16–21. <https://doi.org/10.1111/j.1151-2916.1976.tb09377.x>.
- [81] G. Adam, J.H. Gibbs, On the Temperature Dependence of Cooperative Relaxation Properties in Glass-Forming Liquids, *J. Chem. Phys.* 43 (1965) 139–146. <https://doi.org/10.1063/1.1696442>.
- [82] G.W. Scherer, Use of the Adam-Gibbs Equation in the Analysis of Structural Relaxation, *J. Am. Ceram. Soc.* 67 (2006) 504–511. <https://doi.org/10.1111/j.1151-2916.1984.tb19643.x>.
- [83] G.W. Scherer, Volume Relaxation Far from Equilibrium, *J. Am. Ceram. Soc.* 69 (1986) 374–381. <https://doi.org/10.1111/j.1151-2916.1986.tb04764.x>.
- [84] J. Tauke, T.A. Litovitz, Macedo, P. B., Viscous Relaxation and Non-Arrhenius Behavior in B₂O₃, *J. Am. Ceram. Soc.* 51 (1968) 158–163. <https://doi.org/10.1111/j.1151-2916.1968.tb11859.x>.
- [85] J.A. Bucaro, H.D. Dardy, R.D. Corsaro, Strain relaxation in glass by optical correlation and pressure jump relaxation, *J. Appl. Phys.* 46 (1975) 741–746. <https://doi.org/10.1063/1.321639>.
- [86] D. Sidebottom, R. Bergman, L. Börjesson, L.M. Torell, Two-step relaxation decay in a strong glass former, *Phys. Rev. Lett.* 71 (1993) 2260–2263. <https://doi.org/10.1103/PhysRevLett.71.2260>.
- [87] D.L. Sidebottom, B. V. Rodenburg, J.R. Changstrom, Connecting structure and dynamics in glass

- forming materials by photon correlation spectroscopy, *Phys. Rev. B.* 75 (2007) 132201. <https://doi.org/10.1103/PhysRevB.75.132201>.
- [88] F. Dallari, B.H. Kintov, G. Pintori, F. Riboli, F. Rossi, C. Armellini, M. Montagna, G. Monaco, The structural relaxation dynamics in the glass-former B₂O₃: A multi-speckle dynamic light scattering study, *Philos. Mag.* 96 (2016) 800–808. <https://doi.org/10.1080/14786435.2016.1147656>.
- [89] A.K. Hassan, L.M. Torell, L. Börjesson, H. Doweidar, Structural changes of B₂O₃ through the liquid-glass transition range: A Raman-scattering study, *Phys. Rev. B.* 45 (1992) 12797–12805. <https://doi.org/10.1103/PhysRevB.45.12797>.
- [90] B. Sales, Structural relaxation dynamics of phosphate glasses: The effects of network topology on the glass transition, *J. Non. Cryst. Solids.* 119 (1990) 136–150. [https://doi.org/10.1016/0022-3093\(90\)90837-C](https://doi.org/10.1016/0022-3093(90)90837-C).
- [91] H.Z. Zhuang, X.W. Zou, Z.Z. Jin, D.C. Tian, Probability model for relaxation, *Phys. Rev. B - Condens. Matter Mater. Phys.* 55 (1997) 14047–14050. <https://doi.org/10.1103/PhysRevB.55.14047>.
- [92] H.-Z. Zhuang, X.-W. Zou, Z.-Z. Jin, D.-C. Tian, Temperature dependence of Raman spectra of vitreous and molten B₂O₃, *Phys. Rev. B.* 55 (1997) R6105–R6108. <https://doi.org/10.1103/PhysRevB.55.R6105>.
- [93] H.Z. Zhuang, X.W. Zou, Z.Z. Jin, D.C. Tian, β and α relaxation in B₂O₃ below and near the glass transition temperature, *Phys. Lett. Sect. A Gen. At. Solid State Phys.* 237 (1998) 253–256. [https://doi.org/10.1016/S0375-9601\(98\)00878-0](https://doi.org/10.1016/S0375-9601(98)00878-0).
- [94] R. Conradt, Modeling of the thermochemical properties of multicomponent oxide melts, *Zeitschrift Für Met.* 92 (2001) 1158–1162.
- [95] R. Conradt, Chemical structure, medium range order, and crystalline reference state of multicomponent oxide liquids and glasses, *J. Non. Cryst. Solids.* 345–346 (2004) 16–23. <https://doi.org/10.1016/j.jnoncrysol.2004.07.038>.
- [96] R. Conradt, The industrial glass melting process, in: K. Hack (Ed.), *SGTE Caseb. Thermodyn. Work*, 2nd ed., Woodhead Publishing Ltd, CRC Press, Cambridge, England, 2008: pp. 282–303.
- [97] B.A. Shakhmatkin, N.M. Vedishcheva, M.M. Shultz, A.C. Wright, The thermodynamic properties of oxide glasses and glass-forming liquids and their chemical structure, *J. Non. Cryst. Solids.* 177 (1994) 249–256. [https://doi.org/10.1016/0022-3093\(94\)90538-X](https://doi.org/10.1016/0022-3093(94)90538-X).
- [98] N.M. Vedishcheva, B.A. Shakhmatkin, A.C. Wright, The structure of sodium borosilicate glasses: Thermodynamic modelling vs. experiment, *J. Non. Cryst. Solids.* 345–346 (2004) 39–44. <https://doi.org/10.1016/j.jnoncrysol.2004.07.040>.
- [99] N.M. Vedishcheva, B. a. Shakhmatkin, A.C. Wright, The Structure-Property Relationship in Oxide Glasses: A Thermodynamic Approach, *Adv. Mater. Res.* 39–40 (2008) 103–110. <https://doi.org/10.4028/www.scientific.net/AMR.39-40.103>.
- [100] I.G. Vedishcheva, Natalia M. Polyakova, A.C. Wright, Short and intermediate range order in sodium borosilicate glasses: a quantitative thermodynamic approach, *Phys. Chem. Glas. - Eur. J. Glas. Sci. Technol. Part B.* 55 (2014) 225–236.
- [101] H.L. Lukas, S.G. Fries, B. Sundman, *Computational Thermodynamics: The Calphad Method*, Cambridge University Press, 2007. <https://doi.org/10.1017/CBO9780511804137>.
- [102] W. Capps, P.B. Macedo, B. O'Meara, T.A. Litovitz, Temperature Dependence of the High Frequency Moduli of Vitreous B₂O₃, *J. Chem. Phys.* 45 (1966) 3431–3438. <https://doi.org/10.1063/1.1728124>.
- [103] R.D. Corsaro, J. Jarzynski, Thermodynamic properties of boron trioxide in the glass transition region, *J. Chem. Phys.* 5128 (1974) 5128–5129. <https://doi.org/10.1063/1.1681040>.
- [104] V.L. Solozhenko, O.O. Kurakevych, Y. Le Godec, V. V. Brazhkin, Thermodynamically Consistent p – T Phase Diagram of Boron Oxide B₂O₃ by in Situ Probing and Thermodynamic Analysis, *J. Phys. Chem. C.* 119 (2015) 20600–20605. <https://doi.org/10.1021/acs.jpcc.5b07088>.
- [105] V. V. Brazhkin, Y. Katayama, K. Trachenko, O.B. Tsiok, A.G. Lyapin, E. Artacho, M. Dove, G. Ferlat, Y. Inamura, H. Saitoh, Nature of the Structural Transformations in B₂O₃ Glass under High Pressure, *Phys. Rev. Lett.* 101 (2008) 035702. <https://doi.org/10.1103/PhysRevLett.101.035702>.

- [106] P.K. Gupta, C.T. Moynihan, Prigogine-Defay ratio for systems with more than one order parameter, *J. Chem. Phys.* 65 (1976) 4136–4140. <https://doi.org/10.1063/1.432870>.
- [107] H.W. Leidecker, J.H. Simmons, T.A. Litovitz, P.B. Macedo, Degenerate Excited State in the Structure of B₂O₃, *J. Chem. Phys.* 55 (1971) 2028–2031. <https://doi.org/10.1063/1.1676369>.
- [108] J. Rault, The Modified VFT law of glass former materials under pressure: Part II: Relation with the equation of state, *Eur. Phys. J. E.* 38 (2015) 1–19. <https://doi.org/10.1140/epje/i2015-15091-6>.
- [109] E. Masiewicz, A. Grzybowski, K. Grzybowska, S. Pawlus, J. Pionteck, M. Paluch, Adam-Gibbs model in the density scaling regime and its implications for the configurational entropy scaling, *Sci. Rep.* 5 (2015) 13998. <https://doi.org/10.1038/srep13998>.